6

MICROSTRIP ANTENNAS

Microstrip antennas are planar resonant cavities that leak from their edges and radiate. We can utilize printed circuit techniques to etch the antennas on soft substrates to produce low-cost and repeatable antennas in a low profile. The antennas fabricated on compliant substrates withstand tremendous shock and vibration environments. Manufacturers for mobile communication base stations often fabricate these antennas directly in sheet metal and mount them on dielectric posts or foam in a variety of ways to eliminate the cost of substrates and etching. This also eliminates the problem of radiation from surface waves excited in a thick dielectric substrate used to increase bandwidth.

As electronic devices continue to shrink in size, the antenna designer is pushed to reduce the antenna size as well. Cavity antennas use valuable internal volume, but we have the conflict that restricting the volume limits impedance bandwidth. Bandwidths widen with increased circuit losses (material losses) or by efficient use of the restricted volume. Bounds on bandwidth can be found by enclosing the antenna in a sphere and expanding the fields into TE and TM spherical modes [1,2]. Each mode radiates, but it requires more and more stored energy as the mode number increases. Decreasing the volume increases the Q value of each mode and a sum, weighted by the energy in each mode, determines the overall Q value. Antennas that use the spherical volume efficiently and reduce power in the higher-order modes have the greatest bandwidths. A single lowest-order mode puts an upper bound on bandwidth, given the size of the enclosing sphere. Greater volumes have potential for greater bandwidth provided that the energy in higher-order spherical modes is restricted. Increasing material losses or adding small resistors increases bandwidth beyond the single-mode bound [2]. We discover that increasing the volume of flush antennas increases the impedance bandwidth provided that the radiation mode on the structure can be maintained. Thicker substrates develop greater bandwidths, but they increase the possibility of higher-order-mode excitation and surface-wave losses. Losses limit the lower bound of bandwidth

Modern Antenna Design, Second Edition, By Thomas A. Milligan

as we reduce the thickness because efficiency degrades to a point where the bandwidth remains constant.

Microstrip consists of a metal strip on a dielectric substrate covered by a ground plane on the other side. Unlike stripline, the single ground plane shields the circuit on only one side, but normal packaged microstrip—within a receiver, for example—has a second shielding ground plane to reduce circuit interactions. The dielectric substrate retains most of the power because the shielding ground plane is spaced a few substrate thicknesses away. Removing the shield in antenna applications allows radiation from resonant cavities. We also discover feeding circuits etched on the substrate radiate to some extent, but their radiation is comparatively small.

Arrays of antennas can be photoetched on the substrate, along with their feeding networks, and microstrip provides easy connections to active devices and allows placement of preamps or distributed transmitters next to the antenna elements. Diode phase-shifter circuits etched in the microstrip form single-board phased arrays. Microstrip circuits make a wide variety of antennas possible through the use of the simple photoetching techniques.

The vast literature on microstrip antennas concentrates on the microwave circuit analysis of the internal parts of the antenna used to control the internal modes. Designers have increased the bandwidth of the antenna by coupling to multiple resonators, such as vertically stacked or coplanar coupled patches or by using internal slots and apertures. These multiple resonators increase the impedance bandwidth, and in the best cases the antenna continues to radiate the same pattern. As antenna designers we need to concentrate first on obtaining the desired pattern while working to increase the impedance bandwidth. Simple microstrip antennas have much larger pattern bandwidths than impedance bandwidths, but as more resonators are added to increase the impedance bandwidth, spreading in the horizontal plane alters the radiated pattern and we must return to concentrate on the pattern.

Microstrip patch antennas consist of metal patches large with respect to normal transmission-line widths. A patch radiates from fringing fields around its edges. Impedance match occurs when a patch resonates as a resonant cavity. When matched, the antenna achieves peak efficiency. A normal transmission line radiates little power because the fringing fields are matched by nearby counteracting fields. Power radiates from open circuits and from discontinuities such as corners, but the amount depends on the radiation conductance load to the line relative to the patches. Without proper matching, little power radiates.

The edges of a patch appear as slots whose excitations depend on the internal fields of the cavity. A general analysis of an arbitrarily shaped patch considers the patch to be a resonant cavity with metal (electric) walls of the patch and the ground plane and magnetic or impedance walls around the edges. The radiating edges and fringing fields present loads along the edges. In one analysis [3] the patch effective size is increased to account for the capacitive susceptance of fringing fields, and the radiation admittance is ignored to calculate resonant frequency. The far field is integrated to compute radiated power and the equivalent radiation conductance. The second method [4] is to retain the patch size but satisfy boundary conditions into a loaded wall whose load is determined by radiation and fringing fields. Assuming a constant electric field from the ground plane to the substrate allows solutions in terms of modes TM to the substrate thickness. Boundary conditions determine possible modes and correspond to the dual TE modes of waveguides having electric walls. Patches in the shape of standard coordinate system

axes, such as rectangular and circular, give solutions in terms of tabulated functions. Numerical techniques used for arbitrarily shaped waveguides can be applied to patches with nonstandard shapes. We consider only rectangular and circular patches.

6-1 MICROSTRIP ANTENNA PATTERNS

We start our discussion of patches with their pattern characteristics. It is difficult to separate a discussion of pattern from the internal construction consideration, but we will only briefly discuss the internal structures that affect the pattern. The small size of microstrip antennas limits control of the pattern and we must use arrays of patches to control its pattern seriously. Rectangular and circular are the most common shapes for microstrip antennas and they radiate similar broad patterns. When we load the cavity to shrink its size, it radiates wider beamwidth patterns that lower directivity (gain). Antennas that couple to coplanar patches to increase the impedance bandwidth will radiate narrower beams, but the basic patch has a wide beamwidth. If we couple to multiple coplanar patches, we can expect the pattern to narrow or vary its shape as the mixture of modes on the various patches changes over the frequency range of operation.

Patches consist of metal plates suspended over large ground planes. We excite the cavity in a variety of ways that we discuss later. Electric currents flow on the plate and on the ground plane around the antenna, and these radiate. If we use vertical probes to excite the antenna from coaxial lines, the currents flowing on these radiate and add to the pattern. We can reduce the antenna size by adding vertical shorting plates (quarter-wave patches) or shorting pins near the feed pins (compact patches), and these also radiate from the current flow on them. Remember that the patch radiates from real electric currents, although the distribution is complicated.

We simplify the problem of computing patch radiation by using magnetic currents along the edges. Figure 6-1 illustrates the fringing electric fields around the edges of square and circular patch antennas excited in the lowest-order cavity modes. The arrow sizes indicate the magnitude of the fields. The square patch has nearly uniform fields along two edges we call the width, and a sinusoidal variation along the other two edges, called the resonant length. The fields vanish along a virtual electrically short-circuited plane halfway across the patches. On either side of the short-circuit plane, the fields are directed in opposite directions. Looking from above the fields along the width, both edges are in the same direction. The circular patch fringing fields distribution varies as $\cos \phi$, where the angle ϕ along the rim is measured from the peak electric field. Magnetic currents found from the fringing electric fields can replace the electric currents located on the patch and the surrounding ground plane for pattern analysis. Figure 6-2 shows the distribution of magnetic currents around the edges, with the size of the arrowhead indicating magnitude.

Our use of magnetic currents around the patch perimeter reduces the pattern calculation to equivalent slots. A two-element array consisting of slots with equivalent uniform magnetic currents produces the E-plane radiation of a rectangular patch. To first order, the slots are spaced $\lambda/2\sqrt{\varepsilon_r}$ and we can determine the pattern from the equivalent two-element array. The magnetic currents along the resonant length sides individually cancel because the current changes direction halfway across the edge. The currents also cancel from side to side. These cancellations eliminate pattern contributions to the E- and H-plane patterns. The slot length determines the H-plane pattern.

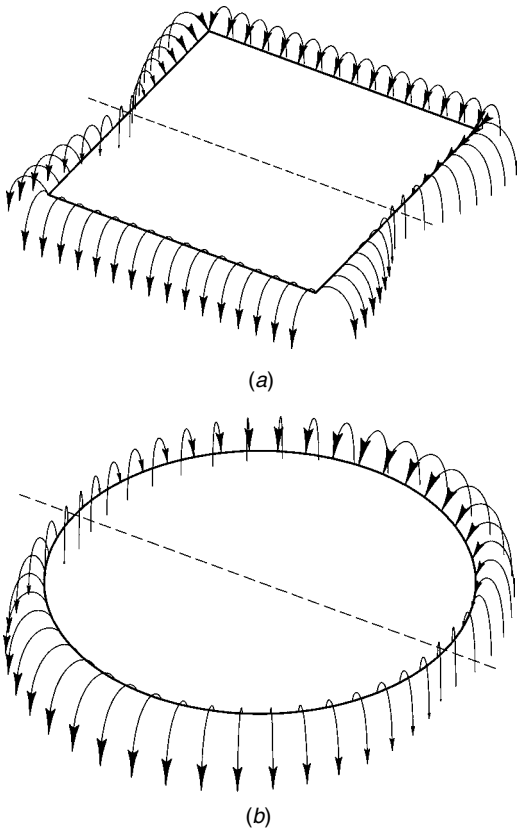

FIGURE 6-1 Fringing electric fields around microstrip patches: (*a*) square; (*b*) circular. (From L. Diaz and T. A. Milligan, *Antenna Engineering Using Physical Optics,* Figs. 3.12 and 3.19, © 1996 Artech House, Inc.).

The H-plane of the slot has the same pattern as the E-plane of a dipole and produces a null along its axis. Figure 6-3 illustrates the pattern of a patch on an infinite ground plane using a free-space substrate. The two-element slot array in the E-plane generates a null along the ground plane because the elements are spaced $\lambda/2$. The H-plane dashed curve shows the null along the ground plane due to the polarization of the slots. The light curves give the Huygens source polarization (Section 1-11.2) patterns in the diagonal planes. The antenna radiates cross-polarization (dashed curve) in this plane from the combination of separated magnetic currents along the resonant-length sides and from the unbalance in the beamwidths in the principal planes.

When we design a microstrip patch on a dielectric substrate, the size reduction brings the two slots closer together and widens the E-plane beamwidth and eliminates its null along the ground plane. Figure 6-4 illustrates the pattern of a patch designed for a substrate with $\varepsilon_r = 2.2$. The H-plane pattern retains its null along the ground plane due to the slot pattern. The cross-polarization of the Huygens source in the diagonal plane increases because of the increased difference between the beamwidths of the principal plane patterns. Table 6-1 gives the directivity of a square and circular patch on an infinite ground plane found by integrating the pattern. The range of directivity

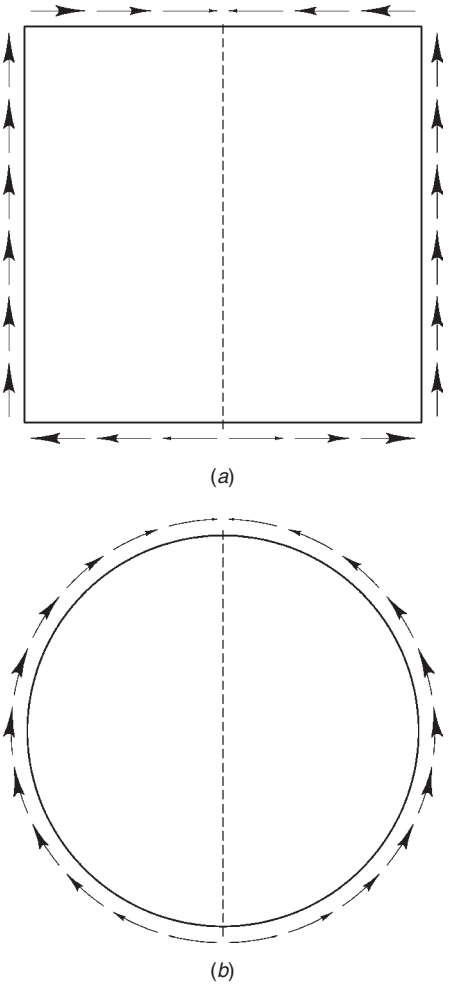

FIGURE 6-2 Equivalent magnetic currents on the edges of microstrip patches: (*a*) square; (*b*) circular.

of a patch is limited. Increasing the width of a rectangular patch increases directivity by shrinking the H-plane beamwidth.

We gain some control of the pattern by placing the patch on a finite ground plane. Figure 6-5 shows the pattern of a square patch on a 2.21 dielectric constant substrate when located on circular disks 5λ, 2λ, and 1λ in diameter. On a 5λ ground plane, edge diffraction adds ripple to the pattern. As the ground plane increases, the angular separation between the ripples decreases, due to the increased array size of the radiation from the two edges. The H-plane pattern widens significantly for 1λ- and 2λ-diameter ground planes, as the limited ground plane can no longer support the currents that make the patch edge radiate like a slot. Although the principal-plane beamwidths are more nearly equal for the patch on the 2λ-diameter disk, the cross-polarization in the diagonal plane increases relative to the pattern on the infinite ground plane. The 1λ ground plane increases the gain of the patch by about 1 dB relative to the patch on an

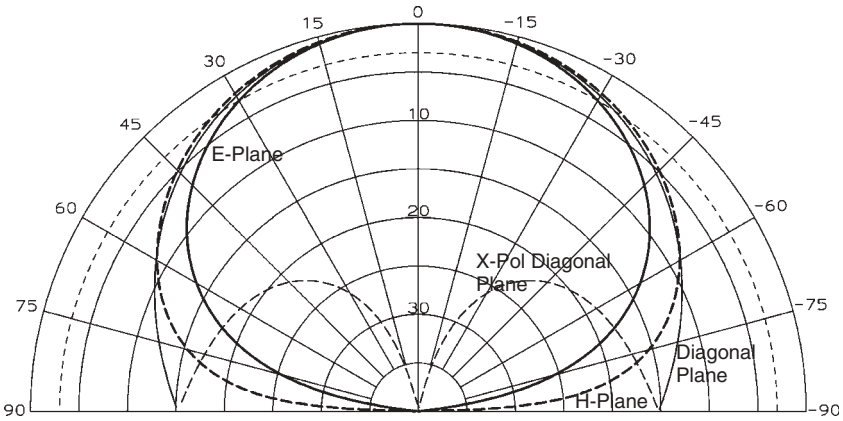

FIGURE 6-3 Patterns of microstrip patch on a free-space substrate mounted on an infinite ground plane.

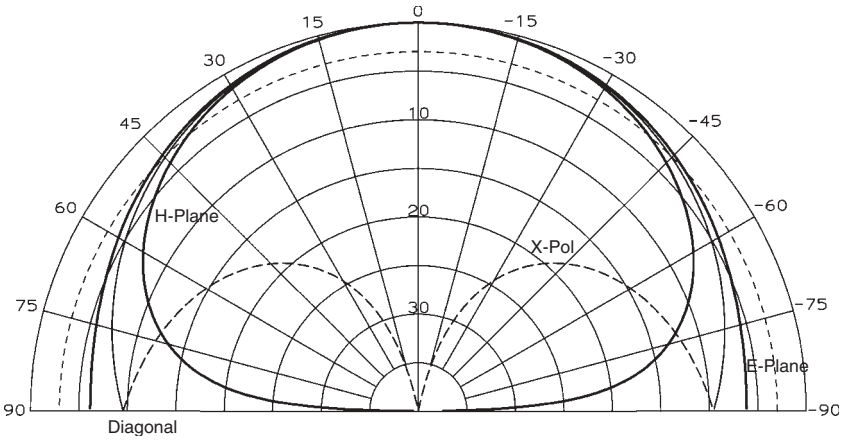

FIGURE 6-4 Patterns of microstrip patch on a dielectric substrate $\varepsilon_r = 2.2$ over an infinite ground plane.

TABLE 6-1 Estimated Directivity of Square and Circular Microstrip Patches on a Large Ground Plane

Dielectric Constant	Square Patch (dB)	Circular Patch (dB)
1.0	8.4	9.8
2.0	7.7	7.6
3.0	7.2	6.7
4.0	7.0	6.2
6.0	6.7	5.8
8.0	6.5	5.5
10.0	6.4	5.4
16.0	6.3	5.1

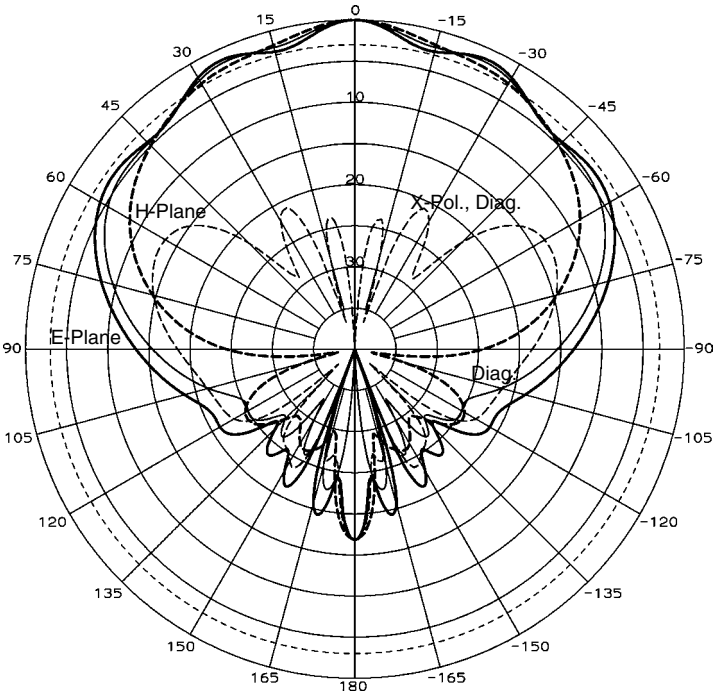

(*a*)

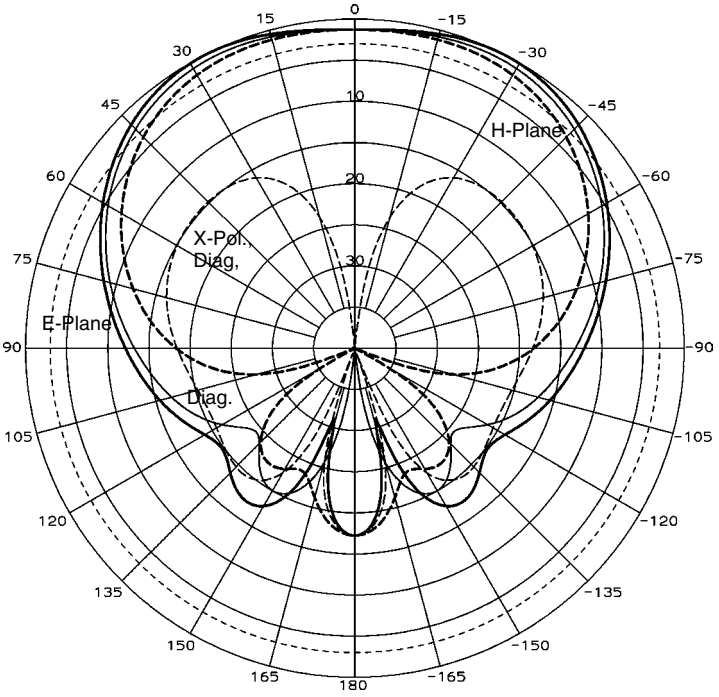

(*b*)

FIGURE 6-5 Patterns of microstrip patches with dielectric substrate $\varepsilon_r = 2.2$ mounted over finite circular ground planes: (*a*) 5λ diameter; (*b*) 2λ diameter. (*continued*)

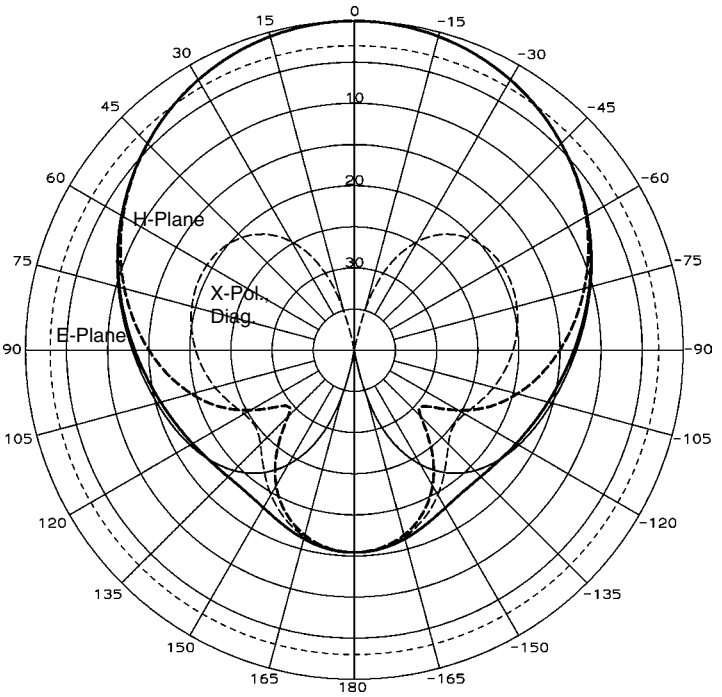

(*c*)

FIGURE 6-5 (*continued*) (*c*) 1λ diameter.

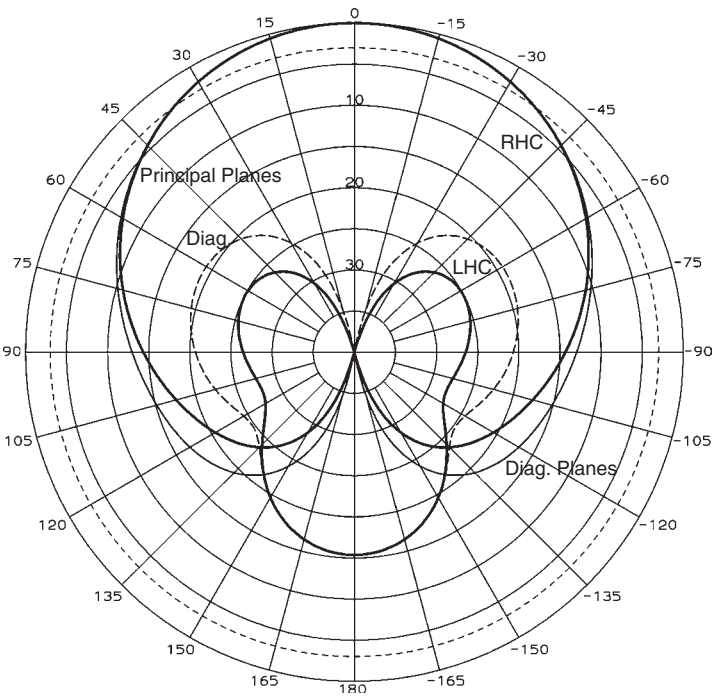

FIGURE 6-6 Circularly polarized patch mounted on a 1λ-diameter ground plane.

infinite ground plane. In this case the edge diffractions add constructively to narrow the beamwidths. We can take advantage of the nearly equal E- and H-plane patterns in the forward hemisphere to produce a pattern with excellent circular polarization over the entire hemisphere when we feed the patch for circular polarization. Figure 6-6 gives the circular polarization pattern when the patch is fed in two spots with equal signals phased 90° apart. The cross-polarization is 13 dB below the co-polarization at $\theta = 90^\circ$ in the principal planes and -7 dB in the diagonal plane. We retain these excellent polarization characteristics over a large ground plane if we place the finite ground plane on a 1λ or greater pedestal above the ground plane.

6-2 MICROSTRIP PATCH BANDWIDTH AND SURFACE-WAVE EFFICIENCY

Microstrip patches radiate from the currents induced on the patch or equivalently, the magnetic currents around the periphery of the patch and from surface waves induced in the dielectric slab. The surface waves radiate when they reach the edges of the substrate and their radiation contributes to the normal patch radiation. The fringing fields from the patch to the ground plane readily excite the lowest-order surface-wave TM_0 mode that has no low frequency cutoff. Any thickness dielectric slab supports this mode. We can control the surface-wave radiation by limiting the substrate area or by adding etched photonic bandgap patterns to the open areas of the substrate, but generally, surface waves are undesirable. As the substrate thickness or dielectric constant increases, the ratio of the power in surface waves increases. When we calculate the microstrip patch antenna impedance bandwidth, we must include the directly radiated power and the surface-wave power. For most cases we consider surface-wave radiation as reducing radiation efficiency, but for a single patch on a substrate with limited area, its radiation can add constructively. We eliminate surface waves by using metal plate patches without dielectric substrates or low-density foam supports of the patch. Surface waves are bound to the dielectric similar to any transmission line except that the field decays exponentially in the direction normal to the surface. Because the surface wave is excited along the finite edges of the patch, it spreads in the horizontal plane. The radiation spreads like a two-dimensional wave and the fields decay as $1/\sqrt{r}$, where r is the horizontal distance from the edge. This is a far-field approximation, and close to the edge it is a near-field problem. Unfortunately, these surface waves increase the coupling between patches fabricated on the same substrate.

Simple formulas have been derived for the impedance bandwidth of rectangular patches that include the surface-wave loss [5]. Since substrates can be both electric and magnetic, we define the index of refraction of a patch substrate that includes both parameters: $n = \sqrt{\varepsilon_r \mu_r}$. The idea is that the ratio of space-wave radiation to surface-wave radiation can be found for any small antenna mounted on the substrate and we can then apply it to a patch. By integrating the power density in the radiation from a horizontal Hertzian (incremental) dipole spaced the substrate thickness over a ground plane, we obtain the space-wave radiated power in closed form given the substrate thickness h and the free-space propagation constant k:

$$P_R^h \simeq k^2 (kh)^2 \cdot 20\,\mu_r^2 C_1$$
$$C_1 = 1 - \frac{1}{n^2} + \frac{0.4}{n^4} \tag{6-1}$$

We express the current on the patch as an integral of Hertzian dipoles. The surface-wave power generated in the substrate by the Hertzian dipole can be simplified when the substrate is thin:

$$P_{\mathrm{SW}}^{h} = k^2(kh)^3 \cdot 15\pi\mu_r^3 \left(1 - \frac{1}{n^2}\right)^3 \tag{6-2}$$

We define the surface-wave radiation efficiency by the ratio of radiated power to total power:

$$\eta_{\mathrm{SW}} = \frac{P_r^h}{P_R^h + P_{\mathrm{SW}}^h} = \frac{4C_1}{4C_1 + 3\pi kh\mu_r(1 - 1/n^2)^3} \tag{6-3}$$

We relate the power radiated by a patch to a Hertzian dipole by integrating the surface current on the patch consisting of a distribution of small dipoles to calculate the total space-wave power of the patch:

$$P_R = P_R^h m_{\mathrm{eq}}^2 = P_R^h \left(\iint_S J_S \, dx \, dy \right)^2 \tag{6-4}$$

For a rectangular patch the ratio of P_R to $P_R^h m_{\mathrm{eq}}^2$, p, can be approximated by a simple formula given the resonant length L, the width W, and the propagation constant k:

$$p = 1 - \frac{0.16605(kW)^2}{20} + \frac{0.02283(kW)^4}{560} - \frac{0.09142(kL)^2}{10} \tag{6-5}$$

The 2 : 1 VSWR of the rectangular patch is related to the quality factor Q that includes the space- and surface-wave radiations:

$$\mathrm{BW} = \frac{1}{\sqrt{2}\ Q} = \frac{16C_1 p}{3\sqrt{2}\ \eta_{\mathrm{SW}}} \frac{1}{\varepsilon_r} \frac{h}{\lambda_0} \frac{W}{L} \tag{6-6}$$

Figure 6-7 plots the 2 : 1 VSWR bandwidth given by Eq. (6-6) for common substrates versus the free-space thickness in wavelengths and includes the radiation due to surface waves. The surface-wave radiation found using Eq. (6-3) becomes a significant part of the total radiation as the substrate thickness increases or the dielectric constant increases, as shown in Figure 6-8 of the surface-wave loss.

For a single resonator circuit model for a patch, Eq. (6-6) computes bandwidth from the Q and the allowable input VSWR:

$$\mathrm{BW} = \frac{\mathrm{VSWR} - 1}{Q\sqrt{\mathrm{VSWR}}} \quad \text{or} \quad Q = \frac{\mathrm{VSWR} - 1}{\mathrm{BW}\sqrt{\mathrm{VSWR}}} \tag{6-7}$$

We determine bandwidth at different VSWR levels by manipulating Eq. (6-7):

$$\frac{\mathrm{BW}_2}{\mathrm{BW}_1} = \frac{(\mathrm{VSWR}_2 - 1)\sqrt{\mathrm{VSWR}_1}}{(\mathrm{VSWR}_1 - 1)\sqrt{\mathrm{VSWR}_2}} \tag{6-8}$$

Quality factor Q is another way of expressing efficiency. The Q used in Eq. (6-6) is the combination of the space-wave radiation Q_R and the surface-wave radiation Q_{SW}:

$$\frac{1}{Q} = \frac{1}{Q_{\mathrm{rad}}} = \frac{1}{Q_R} + \frac{1}{Q_{\mathrm{SW}}} = \frac{P_R + P_{\mathrm{SW}}}{\omega W_T}$$

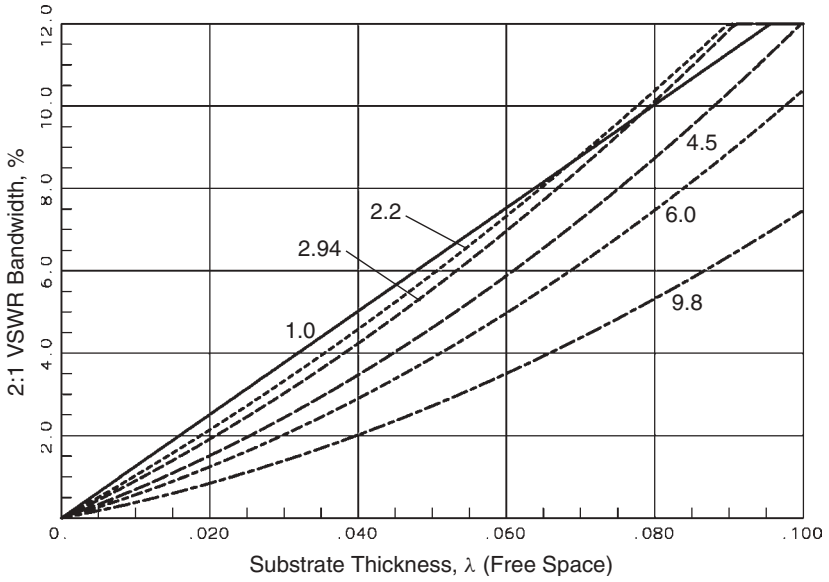

FIGURE 6-7 2:1 VSWR bandwidth of square microstrip patches versus substrate thickness in free-space wavelengths, including surface-wave radiation.

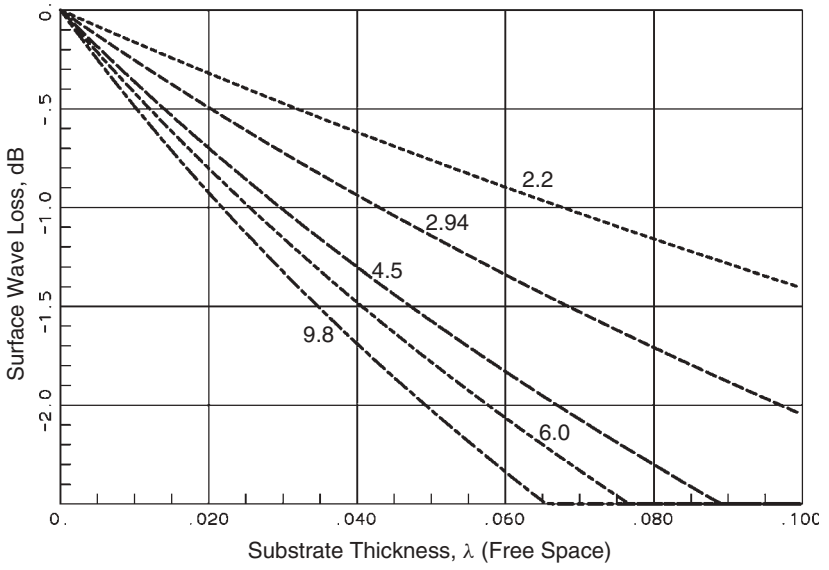

FIGURE 6-8 Surface-wave loss of microstrip patches versus substrate thickness for common substrate dielectric constants.

W_T is the energy stored in the patch and the surface wave and $\omega = 2\pi f$, the radian frequency. Equation (6-3) can be expressed in terms of Q:

$$\eta_{\text{SW}} = \frac{Q}{Q_R} = \frac{Q_{\text{rad}}}{Q_R}$$

The surface wave is not a dissipation loss, but potentially an uncontrolled radiation. Dielectric and conductor losses increase the impedance bandwidth of the patch, but reduce its gain. We express these losses as Q to compute patch efficiency. Given the dielectric loss tangent, $\tan\delta$, and the patch conductivity σ, we have two more Q terms that reduce the overall Q of the patch in terms of impedance bandwidth:

$$Q_d = \frac{1}{\tan\delta} \quad \text{and} \quad Q_c = h\sqrt{\pi f \mu_0 \sigma} \tag{6-9}$$

The total quality factor Q_T is found from the sum of the inverses:

$$\frac{1}{Q_T} = \frac{1}{Q_R} + \frac{1}{Q_{\text{SW}}} + \frac{1}{Q_d} + \frac{1}{Q_c} \tag{6-10}$$

If we attempt to fabricate a patch on a thin substrate, Q_d and Q_c become commensurate with the radiation Q_{rad} and efficiency suffers. The impedance bandwidth increases due to the dissipation in the microstrip patch. Figure 6-7 does not include these losses.

Dielectric Slab Surface Wave We consider the dielectric slab surface wave because it can be excited not only by a microstrip patch but by any wave that passes across it. The slab binds a portion of the wave and releases it when it diffracts at its edges. The surface-wave device slows the wave velocity of this wave relative to the space-wave signal, and when it radiates from the edges it no longer adds in phase with the space wave. The surface-wave fields decrease exponentially in the direction normal to the surface, and the exponential rate increases as the binding increases and the wave propagates more slowly.

A dielectric slab on a ground plane will support TM modes when thin and TE modes when thick. The TM mode is polarized normal to the slab surface, whereas the TE mode is polarized parallel to the slab surface. A TM mode requires an inductive surface such as a corrugated ground plane to bind the wave. While corrugations prevent propagation between the slots, the wave propagates in the dielectric slab by bouncing between the two interfaces at an angle with respect to the surfaces. The second surface can be either free space or a conductor. To solve for the fields, we equate not only the wave impedance at the boundary but the propagation constants in the two regions as well.

We deduce the grounded dielectric slab solution from a slab twice as thick in free space that has an odd-mode electric field excitation on the slab sides. The center becomes a virtual short circuit for the odd-mode excitation. We divide the space around the slab into three regions: 1 above the slab, 2 in the slab, and 3 below the slab and then derive the fields from potential functions [6, p. 129]:

$$\begin{aligned}
\psi_1 &= A_1 \exp\left(\frac{-2\pi b x}{\lambda}\right) \exp(-jk_z z) \\
\psi_2 &= A_2 \begin{Bmatrix} \sin \dfrac{2\pi p_x x}{\lambda} \\ \cos \dfrac{2\pi p_x x}{\lambda} \end{Bmatrix} \exp(-jk_z z) \\
\psi_3 &= \pm A_1 \exp\left(\frac{2\pi b x}{\lambda}\right) \exp(-jk_z z)
\end{aligned} \tag{6-11}$$

where the sign of ψ_3 depends on satisfying continuous tangential fields across the lower slab boundary. The center of the coordinate normal to the slab (x) is the slab center. Equating the propagation constants and x-directed wave impedances produces transcendental equations in the transverse propagation constant in the slab p_x:

$$\sqrt{\left(\frac{\omega a}{2}\right)^2(\varepsilon_1\mu_1-\varepsilon_0\mu_0)-\left(\frac{\pi p_x a}{\lambda}\right)^2}=\pm B_0\frac{\pi p_x a}{\lambda}\left\{\begin{matrix}\tan\dfrac{\pi p_x a}{\lambda}\\ \cot\dfrac{\pi p_x a}{\lambda}\end{matrix}\right\} \tag{6-12}$$

where $B_0=\mu_0/\mu_1$ for TE waves. $B_0=\varepsilon_0/\varepsilon_1$ for TM waves, ω is the radian frequency ($2\pi f$), a is the slab thickness, and ε_1 and μ_1 are the permittivity and permeability of the slab. We solve for p_x [Eq. (6-12)] numerically or graphically and use

$$\frac{\pi b}{\lambda}a=\sqrt{\left(\frac{\omega a}{2}\right)^2(\varepsilon_1\mu_1-\varepsilon_0\mu_0)-\left(\frac{\pi p_x}{\lambda}\right)^2} \tag{6-13}$$

to determine attenuation constant b and the relative propagation constant P of the slab surface wave:

$$k_z=Pk=k\sqrt{1+b^2}\quad\text{or}\quad P=\sqrt{1+b^2} \tag{6-14}$$

For the TM_0 mode we can use an approximate expression for P instead of solving Eq. (6-12) numerically when the slab is thin [7]:

$$P^2=1+\frac{(\varepsilon_r\mu_r-1)^2}{(\varepsilon_r\mu_r)^2}(2ka)^2 \tag{6-15}$$

Equation (6-12) has an infinite number of solutions, corresponding to the multiple values of the tangent and cotangent functions. Order 0 corresponds to the tangent function from 0 to 90°; order 1 corresponds to the cotangent function from 90 to 180°; and so on. Even-mode orders use the tangent function, and odd-mode orders use the cotangent function. We define the cutoff frequency as the point where $\alpha=0$, the transition between attached and detached waves:

$$\lambda_c=\frac{2a}{n}\sqrt{\frac{\varepsilon_1\mu_1}{\varepsilon_0\mu_0}-1} \tag{6-16}$$

The cutoff frequency for the zeroth-order mode is zero. Only the TM_0 mode has odd symmetry, required for the grounded slab. The grounded slab supports even-order TM modes and odd-order TE modes. Equation (6-12) coupled to Eq. (6-13) has been solved numerically to generate Tables 6-2 and 6-3. Table 6-4 lists the thicknesses of a slab in free space supporting the TM_0 mode for a given P. The grounded slab is one-half the thickness of the values in Table 6-2. Similarly, Table 6-3 lists the thicknesses for the TE_1 mode. Equation (6-16) can be solved for the minimum thickness to support the TE_1 mode. Below that thickness the waves do not bind to the surface.

Besides microstrip patches, we feed these surfaces from either a small horn or a parallel-plate transmission line. We match the feed polarization to the mode on the slab, but the slab binds only part of the power. The rest radiates directly from the feed or reflects to the feed input. We can feed an ungrounded slab by centering it in a waveguide. The TE_{10} waveguide mode excites the TE_0 slab mode when the mode velocity determining thickness is in the H-plane. Like the grounded slab with the TM_0

TABLE 6-2 Thickness (λ_0) of a Dielectric Slab Supporting a TM_0 Mode[a]

	Dielectric Constant				
P	2.21	2.94	4.50	6.00	9.80
1.001	0.02699	0.02152	0.01831	0.01839	
1.002	0.03672	0.03041	0.02574	0.02420	
1.005	0.05792	0.04784	0.04032	0.03744	0.03446
1.01	0.08162	0.06713	0.05623	0.05195	0.04710
1.02	0.1147	0.09355	0.07746	0.07094	0.06316
1.04	0.1607	0.1289	0.1046	0.09444	0.08180
1.06	0.1956	0.1545	0.1231	0.1099	0.09331
1.08	0.2253	0.1752	0.1374	0.1215	0.1015
1.10	0.2520	0.1930	0.1491	0.1307	0.1078
1.12	0.2770	0.2088	0.1590	0.1384	0.1129
1.14	0.3012	0.2233	0.1677	0.1450	0.1171
1.16	0.3251	0.2369	0.1756	0.1508	0.1208
1.18	0.3493	0.2499	0.1827	0.1560	0.1240
1.20	0.3741	0.2625	0.1894	0.1607	0.1269
1.25	0.4426	0.2934	0.2045	0.1712	0.1329
1.30	0.5282	0.3250	0.2182	0.1803	0.1380
1.35	0.6492	0.3593	0.2314	0.1887	0.1424
1.40		0.3986	0.2444	0.1966	0.1463

[a] Use half-thickness for a slab on a ground plane.

TABLE 6-3 Thickness (λ_0) of a Dielectric Slab Supporting a TE_1 Mode[a]

	Dielectric Constant				
P	2.21	2.94	4.50	6.00	9.80
1.001	0.4469	0.3689	0.2743	0.2260	0.1701
1.002	0.4720	0.3709	0.2774	0.2272	0.1705
1.005	0.4829	0.3765	0.2770	0.2302	0.1717
1.01	0.4961	0.3843	0.2810	0.2330	0.1736
1.02	0.5164	0.3962	0.2873	0.2373	0.1761
1.04	0.5494	0.4150	0.2968	0.2438	0.1797
1.06	0.5790	0.4313	0.3049	0.2492	0.1825
1.08	0.6078	0.4465	0.3122	0.2540	0.1851
1.10	0.6368	0.4613	0.3191	0.2585	0.1874
1.15	0.7140	0.4982	0.3356	0.2690	0.1928
1.20	0.8046	0.5372	0.3518	0.2790	0.1978
1.25	0.9182	0.5802	0.3683	0.2890	0.2026
1.30	1.0712	0.6291	0.3856	0.2992	0.2073

[a] Use half-thickness for a slab on a ground plane.

mode, the TE_0 mode has no cutoff frequency for a free-space slab. Table 6-4 lists the slab thicknesses for a given relative propagation constant for the TE_0 mode.

The surface-wave power was found in terms of the relative propagation constant P[7]:

$$P_{SW} = \frac{15\pi k^2 n^2 \mu_r^3 (P^2 - 1)}{n^2 \left(\dfrac{1}{\sqrt{P^2 - 1}} + \dfrac{\sqrt{P^2 - 1}}{n^2 - P^2} \right) + kh \left[1 + \dfrac{n^4 (P^2 - 1)}{n^2 - P^2} \right]} \tag{6-17}$$

TABLE 6-4 Thickness (λ_0) of a Dielectric Slab Supporting a TE_0 Mode

	Dielectric Constant				
P	2.21	2.94	4.50	6.00	9.80
1.001	0.01274	0.00994			
1.002	0.01684	0.01174	0.00661	0.00410	0.00250
1.005	0.02649	0.01666	0.00920	0.00638	0.00364
1.01	0.03772	0.02341	0.01289	0.00905	0.00514
1.02	0.05409	0.03345	0.01846	0.01286	0.00729
1.04	0.07872	0.04823	0.02640	0.01839	0.01040
1.06	0.09935	0.06027	0.03275	0.02276	0.01284
1.08	0.1184	0.07104	0.03832	0.02656	0.01494
1.10	0.1368	0.08113	0.04343	0.03002	0.01684
1.15	0.1833	0.1051	0.05507	0.03779	0.02106
1.20	0.2348	0.1290	0.06595	0.04489	0.02483
1.25	0.2968	0.1542	0.07661	0.05168	0.02835

We combine Eq. (6-1) for the space-wave power with Eq. (6-17) for the surface-wave power to calculate efficiency in the same manner as Eq. (6-3). The results are similar.

6-3 RECTANGULAR MICROSTRIP PATCH ANTENNA

Although design equations will be given below for single-layer rectangular and circular patches, serious design work should use one of the excellent available commercial design codes [8]. Their use reduces the need to modify the final dimensions using a knife to remove metal or metal tape to increase the patches. Antennas can be built with tuning tabs, but the labor to trim these increases cost. Tuning tabs are unsuitable for arrays when the input port to individual antennas cannot be accessed. As we add layers to increase bandwidth, a cut-and-try method becomes extremely difficult, and numerical methods are a necessity.

Rectangular patch antennas can be designed by using a transmission-line model [9] suitable for moderate bandwidth antennas. Patches with bandwidths of less than 1% or greater than 4% require a cavity analysis for accurate results, but the transmission-line model covers most designs. The lowest-order mode, TM_{10}, resonates when the effective length across the patch is a half-wavelength. Figure 6-9 demonstrates the patch fed below from a coax along the resonant length. Radiation occurs from the fringing fields. These fields extend the effective open circuit (magnetic wall) beyond the edge. The extension is given by [10]

$$\frac{\Delta}{H} = 0.412 \frac{\varepsilon_{\text{eff}} + 0.300}{\varepsilon_{\text{eff}} - 0.258} \frac{W/H + 0.262}{W/H + 0.813} \tag{6-18}$$

where H is the substrate thickness, W the patch nonresonant width, and ε_{eff} the effective dielectric constant of a microstrip transmission line the same width as the patch.

A suitable approximation for ε_{eff} is given by [11]

$$\varepsilon_{\text{eff}} = \frac{\varepsilon_r + 1}{2} + \frac{\varepsilon_r - 1}{2} \left(1 + \frac{10H}{W}\right)^{-1/2} \tag{6-19}$$

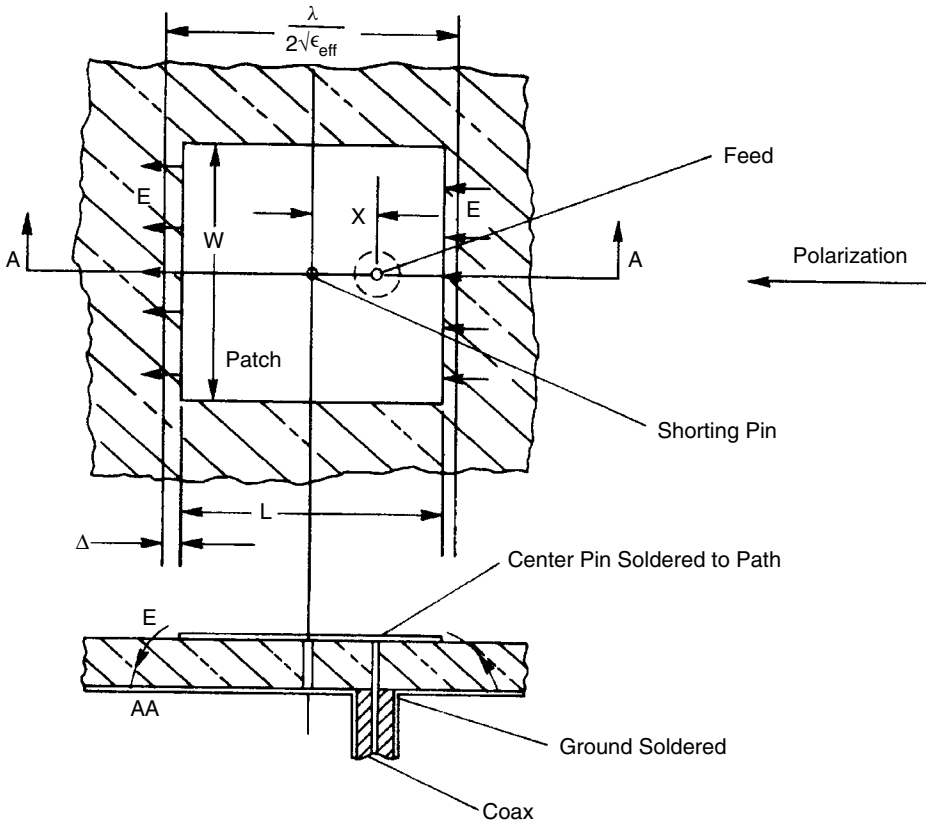

FIGURE 6-9 Coax-fed microstrip patch antenna.

where ε_r is the substrate dielectric constant. The transmission-line model represents the patch as a low-impedance microstrip line whose width determines the impedance and effective dielectric constant. A combination of parallel-plate radiation conductance and capacitive susceptance loads both radiating edges of the patch.

Harrington [6, p. 183] gives the radiation conductance for a parallel-plate radiator as

$$G = \frac{\pi W}{\eta \lambda_0}\left[1 - \frac{(kH)^2}{24}\right] \tag{6-20}$$

where λ_0 is the free-space wavelength. The capacitive susceptance relates to the effective strip extension:

$$B = 0.01668\frac{\Delta}{H}\frac{W}{\lambda}\varepsilon_{\text{eff}} \tag{6-21}$$

Example Design a square microstrip patch antenna at 3 GHz on a 1.6-mm substrate with a dielectric constant of 2.55 (woven Teflon fiberglass). The patch will be approximately a half-wavelength long in the dielectric.

Assume at first that the width is λ/2.

$$W = \frac{c}{2f\sqrt{\varepsilon_r}} = 31.3\,\text{mm}$$

By Eq. (6-19), $\varepsilon_{\text{eff}} = 2.405$. On substituting that value into Eq. (6-18), we obtain the effective cutback on each edge; $\Delta = 0.81\,\text{mm}$. The resonant length is

$$L = \frac{c}{2f\sqrt{\varepsilon_{\text{eff}}}} - 2\Delta = 30.62\,\text{mm}$$

When we use this length as the width (square patch) to calculate the effective dielectric constant, we obtain 2.403, very close to the initial value. We can iterate it once more and obtain 30.64 mm for the resonant length. The input conductance of the patch fed on the edge will be twice the conductance of one of the edge slots [Eq. (6-20)]:

$$G = \frac{30.64\,\text{mm}}{120(100\,\text{mm})}\left\{1 - \frac{[2\pi(1.6)/100]^2}{24}\right\} = 2.55\,\text{mS}$$

$$R = \frac{1}{2G} = 196\,\Omega$$

A microstrip feeding line can be attached to the center of one of the radiating edges but 50-Ω transmission lines become inconveniently wide on low-dielectric-constant substrates. More convenient, 100-Ω narrower lines have about the same low loss and are generally used in feed networks. To transform the 196-Ω input resistance of the example above to 100 Ω, we use a 140-Ω quarter-wavelength transformer. The bandwidth of the transformer far exceeds that of the antenna.

In the example above, we have a square patch. Why doesn't the antenna radiate from the other two edges? We can equally well say that the patch is a transmission line in the other direction. The equal distances from the feed point to the nonradiating edges produce equal fields from the patch to ground. Equal fields on the edges set up a magnetic wall (virtual open circuit) through the centered feed line and create a poor impedance match to the feed.

We expand the radiating edge fields in an odd mode, since the power traveling across the patch loses 180° of phase. The odd mode places a virtual short circuit halfway through the patch. A shorting pin through the center (Figure 6-9) has no effect on radiation or impedance, but it allows a low-frequency grounding of the antenna. The patch can be fed by a coax line from underneath (Figure 6-9). The impedance varies from zero in the center to the edge resistance approximately as

$$R_i = R_e \sin^2 \frac{\pi x}{L} \qquad 0 \le x \le \frac{L}{2} \tag{6-22}$$

where R_i is the input resistance, R_e the input resistance at the edge, and x the distance from the patch center. The feed location does not significantly affect the resonant frequency. By using Eq. (6-22), we locate the feed point given the desired input impedance:

$$x = \frac{L}{\pi} \sin^{-1} \sqrt{\frac{R_i}{R_e}} \tag{6-23}$$

Compute the 50-Ω feed point in the example above:

$$x = \frac{30.64}{\pi} \sin^{-1} \sqrt{\frac{50}{196}} = 5.16\,\text{mm}$$

The feed pin currents add to the pattern by radiating a monopole pattern. Figure 6-10 shows this radiation for a patch using a free-space substrate where the E-plane radiating edges are spaced $\lambda/2$. The pattern of Figure 6-10 has a null along the ground plane in the E-plane, but the monopole radiation increases the radiation along the ground plane. On one side the radiation adds and on the other it subtracts from the E-plane pattern to form a null tilted above the ground plane. The H-plane pattern now contains cross-polarization. We can reduce the monopole radiation by feeding the patch at a second port located an equal distance from the center on the opposite side. This requires an external feed network that divides the power equally between the two ports with a 180° phase difference. The problem with this feed arrangement is that significant power is coupled between the two feeds in the equivalent microwave circuit of the patch. The estimated value of −6 dB coupling between the ports causes a portion of the input power to be dissipated in the second port. At this level the patch efficiency drops 1.25 dB. We can reduce the monopole radiation by coupling to a second short-circuited probe to the patch instead of directly feeding it. The gap between the second probe and the patch is adjusted until the antenna radiates minimum cross-polarization in the H-plane. This uses the microstrip patch as the feed network, and the second probe has no resistive load to dissipate power.

The feed probe across the microstrip patch substrate is a series inductor at the input. Higher-order modes excited in the patch by this feeding method add to the inductive component of the antenna. Below resonance, the antenna is inductive and has near-zero resistance. As the frequency increases, the inductance and resistance grow as the parallel resonance is approached. Above the resonant frequency, the antenna is capacitive as the impedance sweeps clockwise around the Smith chart (Figure 6-11) and finally back to a slight inductive component near a short circuit. Increasing the

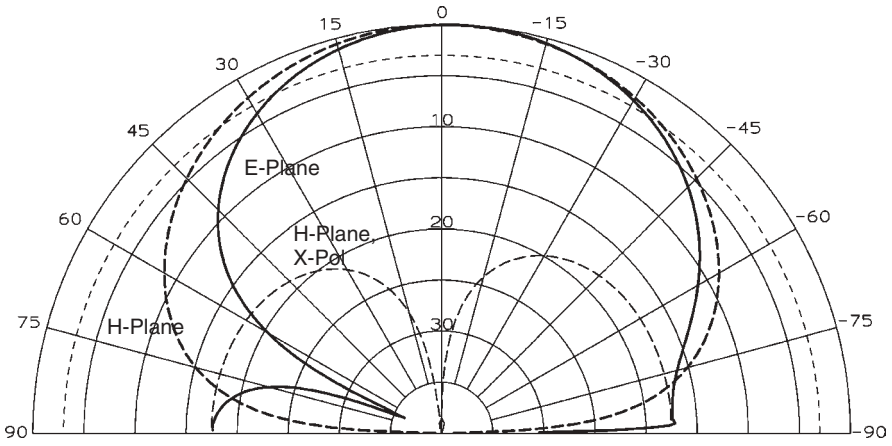

FIGURE 6-10 Pattern of coax-fed, microstrip patch including feed pin radiation for free-space substrate.

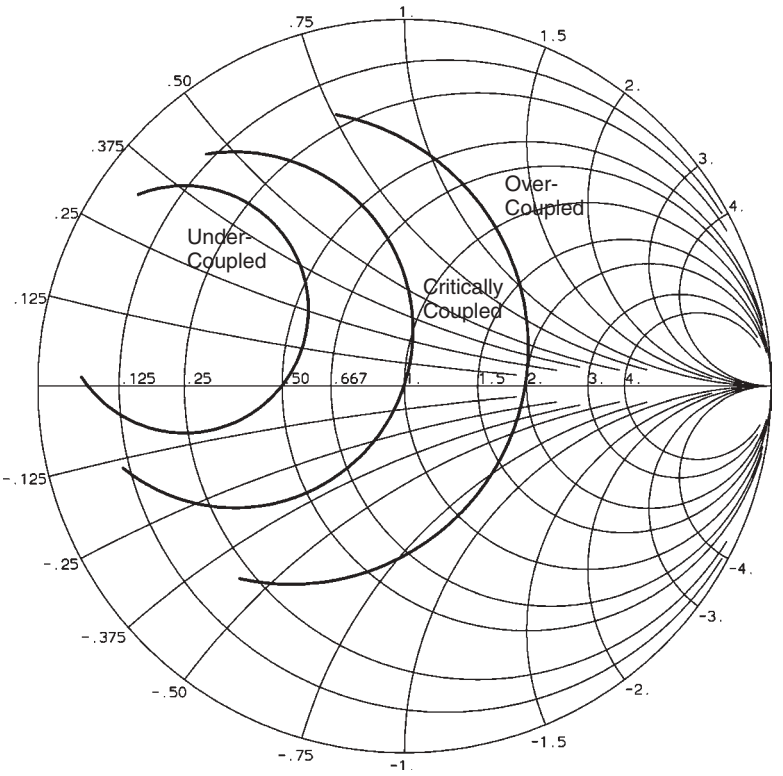

FIGURE 6-11 Smith chart frequency response of under-, critically, and overcoupled patches as the feed point moves toward one radiating edge of a rectangular patch.

input resistance by changing the feed point causes the resonant frequency response circle to grow on the Smith chart and cross the resistance line at a higher level. We call the left-hand curve the undercoupled case because the sweep of the curve fails to enclose the center of the chart. The center curve is critically coupled and the right curve is the overcoupled case. This general impedance response also holds for circular patches. We use these terms for all resonance curves when they sweep around or toward the Smith chart center from any peripheral point.

Figure 6-12 plots the Smith chart for a design with a patch on a 0.05λ-thick substrate with dielectric constant 1.1 that includes the inductance of the feed pin. The response locus lies above the real axis and is always inductive. We can tune this impedance locus by adding a series capacitor at the input with a reactance $-j50$ at the center frequency. The series capacitor moves the locus down until it sweeps around the center of the chart in an overcoupled response. Figure 6-13 shows implementation of the capacitor as a disk on the end of the feed pin. The pin passes through a hole in the patch so that the only connection is through the capacitor disk. The disk can be placed below the patch on a separate substrate in a multiple-layer construction. Other configurations use an annular ring capacitor etching in the patch at the feed point for small capacitors. Adding to this a series inductor and adjusting the series capacitor improves the impedance match over a larger frequency range, as shown in Figure 6-14, where the locus encircles the origin [12]. The patch with the single added

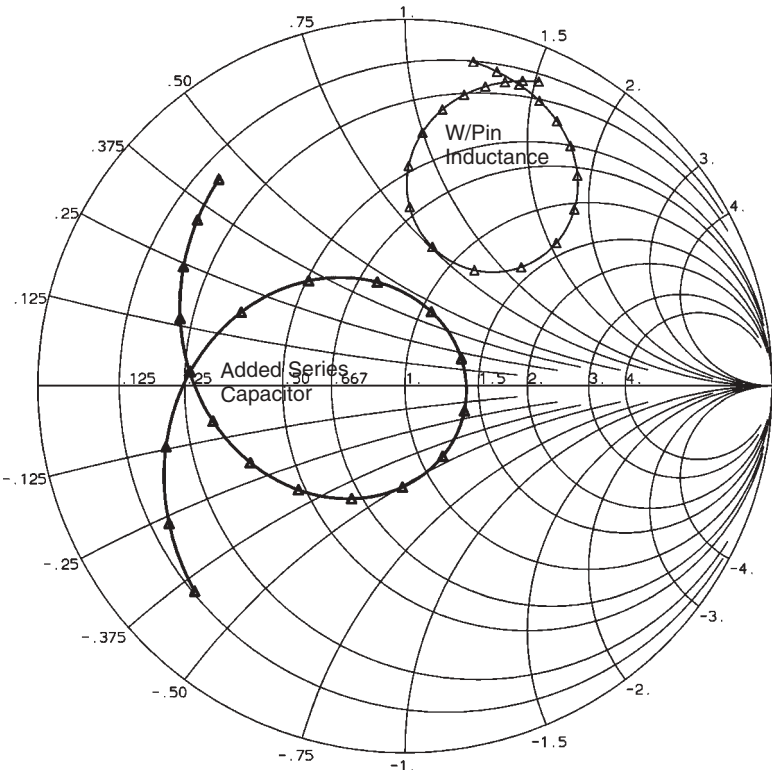

FIGURE 6-12 Impedance improvement by adding a series capacitor to a patch on a thick substrate.

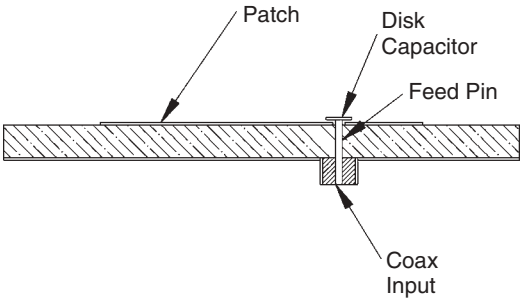

FIGURE 6-13 Cross section of a probe-fed patch with an added series capacitor.

series capacitor has a 9.1% 10-dB return-loss bandwidth while adjusting the series capacitor, and adding a series inductor increases the impedance bandwidth to 15.4%. Matching networks have limited ability to add resonances to broadband the impedance match, but construction becomes difficult. Later, we will obtain extra resonances by adding antenna elements.

We can feed patches from the edge by using an inset microstrip line as shown in Figure 6-15, where the gap on either side of the microstrip line equals its width. A FDTD analysis shows that the inset disturbs the transmission line or cavity model

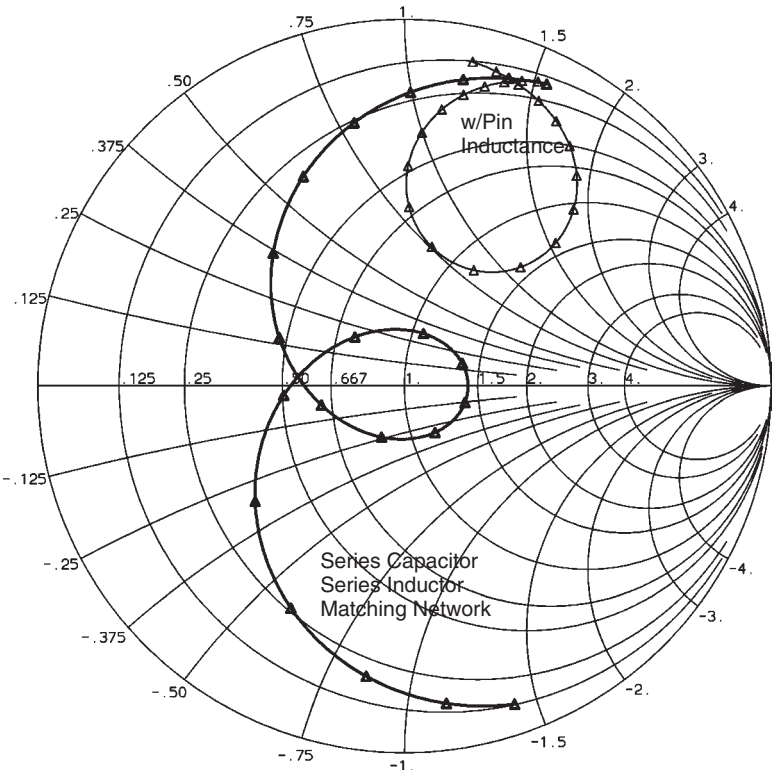

FIGURE 6-14 Impedance response of a patch with a two-element matching network.

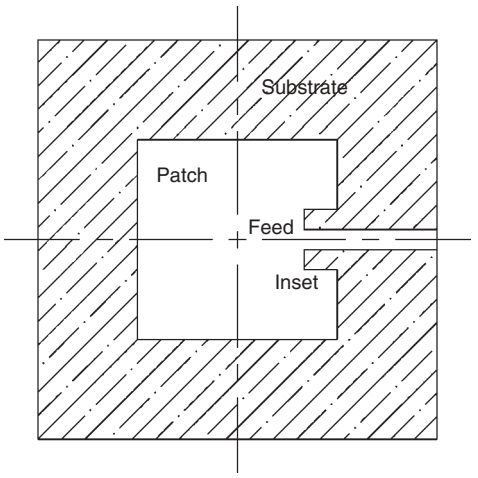

FIGURE 6-15 Inset-fed square patch.

and increases the impedance variation with distance compared to a coaxial probe feed given a patch resonant length L and feed position x from the center [13]:

$$R_i = R_e \sin^4 \frac{\pi x}{L} \qquad 0 \le x \le \frac{L}{2} \tag{6-24}$$

Equation (6-24) is an approximate solution because at $x = 0$, the resistance remains finite. We locate the feed from the equation using a radian angle measure:

$$x = \frac{L}{\pi} \sin^{-1} \left(\frac{R_i}{R_e} \right)^{1/4} \tag{6-25}$$

Compute the 50-Ω feed point in the example above:

$$x = \frac{30.64}{\pi} \sin^{-1} \left(\frac{50}{196} \right)^{0.25} = 7.71 \text{ mm}$$

The inset distance (7.3 mm) is less than the distance of the probe (9.8 mm) from the edge.

Aperture Feed [14,15] A microstrip patch is a planar resonant cavity with open-circuited sidewalls that leak power in radiation. We can also think of the rectangular patch operating in the lowest-order mode as a low-impedance transmission line with end susceptance and radiation conductance. Both models predict a resonant structure with significant Q. Resonant cavities are readily excited by coupling to a transmission line through an aperture or by direct feeding from a transmission line. The Q of the resonant cavity limits the excitation fields to one of the modes. We can expand the excitation in the cavity modes, but the lowest-order mode is usually the most significant and contains most of the stored energy. We generally consider the voltage distribution in a patch with its null plane located halfway across the patch through the center. Whether we consider it as a cavity or a transmission line the standing-wave voltage has a standing-wave current associated with it. This current is out of phase with the voltage and its peak occurs along the virtual short circuit through the centerline. Along the resonant length the current has a cosinusoidal distribution that vanishes at the radiating edges in a single half-cycle for the lowest-order mode. The current has a uniform distribution along the patch width.

We produce maximum coupling to a patch through a slot by distorting the currents in the ground plane of the patch where they are maximum in the center of the patch. To first order the currents flow along the resonant length. This means that we align the slot perpendicular to the current flow for maximum excitation in the same manner as slots in waveguides (Section 5-24). To excite the slot we pass a microstrip transmission line across it perpendicularly. This leads to a three-layer structure. The patch is located on the top layer. Its ground plane contains a coupling aperture usually placed under the center of the patch for maximum coupling. The third layer contains a microstrip transmission using the same ground plane as the patch and located under the center of the slot to maximize coupling. Figure 6-16*a* shows an exploded view of the patch, ground with its aperture, and the microstrip transmission line flipped over relative to the patch. Figure 6-16*b* gives the general parameters associated with the slot aperture. Although x_{os} and y_{os} are usually zero to maximize coupling, the patch current distribution tells us how the coupling varies with slot location. Because the current in the ground plane is uniform across the patch width W, coupling is independent of x_{os} until the slot starts to overlap the edge of the patch. The cosinusoidal distribution current distribution along the resonant length direction L means that the coupling falls off slowly as y_{os} is moved off zero. The sign of y_{os} does not matter because the distribution is an even function. The slow variation of current near the patch center means that the slot location has a loose tolerance.

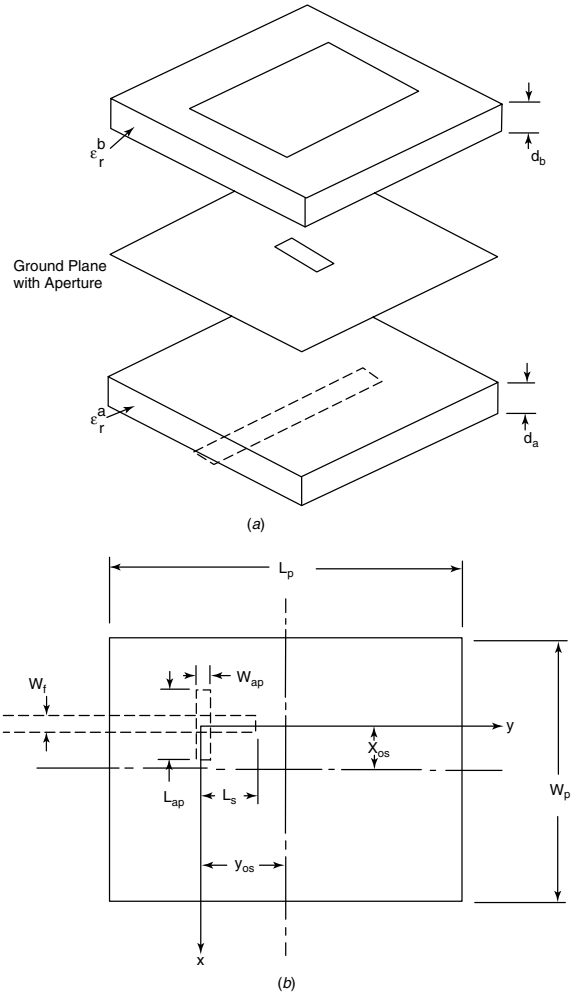

FIGURE 6-16 Aperture feed of square patch. (From [15], Fig. 1, © 1986 IEEE.)

The microstrip transmission line excites the slot (aperture) from a standing-wave with its maximum current located at the slot. We maximize the standing-wave current by either using a shorting via from the microstrip line to the ground plane or by using a quarter-wave open-circuited transmission line stub of length L_s. L_s will be less than a quarter-wave in the effective dielectric constant of the microstrip line because the open-circuit end has fringing capacitance and its capacitance must overcome the higher-order modes of the microstrip patch, which load the input inductively. The reactance of the stub, a series load to the input, is given by the equation

$$Z_S = -jZ_0 \cot(k_{\text{eff}} L_S)$$

where Z_0 is the characteristic impedance of the microstrip feed line, k_{eff} the effective propagation constant in the microstrip substrate, and L_s the stub length $\approx 0.22\lambda_{\text{eff}}$.

We increase the coupling to the patch resonant cavity by increasing the aperture size. Figure 6-17 shows the Smith chart variation with aperture size as the coupling

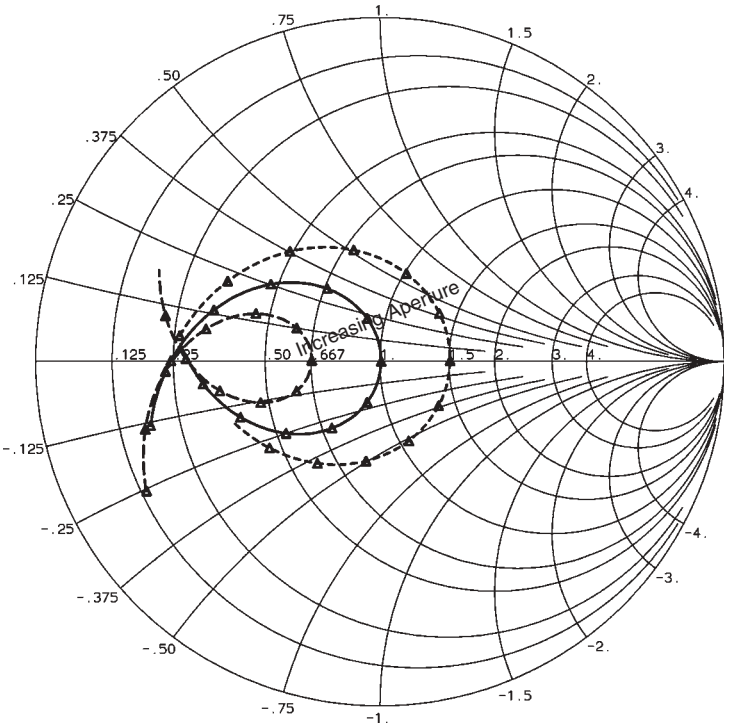

FIGURE 6-17 Effect of aperture size on coupling to a patch where larger openings move the response to the right.

varies left to right as undercoupled, critically coupled, and overcoupled. When we increase the bandwidth, we lower the Q, and the coupling aperture size must increase. Waterhouse [8] suggests starting with a slot about one-half the patch width and using a commercial code to analyze the response while adjusting dimensions before fabrication. We control the rotational position on the Smith chart by varying the open-circuited stub length. Shorter lengths, below $\lambda/4$, increase the capacitive reactance and the coupling loop will rotate around a constant-resistance circle with its diameter determined by the aperture size, as shown in Figure 6-18.

Figure 6-19 gives aperture shapes in order of increasing coupling. The longer slot of (*b*) compared to slot (*a*) increases coupling. Widening the aperture as in (*c*) increases coupling relative to (*a*). The H-shaped slot has a more uniform distribution along the horizontal slot and increased coupling. The bowtie and hourglass apertures increase coupling from a consideration of increased path length around the opening. The smooth curve of the hourglass reduces current discontinuities at the edges and increases coupling [16, pp. 158–159].

Aperture feeding eliminates the vertical pin structure in the microstrip patch and eases construction but at the cost of a multiple-layer etching. The elimination of the vertical pin removes the added monopole pattern, which increases cross-polarization. When the patch is edge fed, whether directly or inset, the substrate for good patch radiation does not match the one needed for good microstrip lines. With an aperture-fed patch, each structure can use its optimum substrate, because they are independent and connected only through the aperture. As we try to feed broadband patches, the

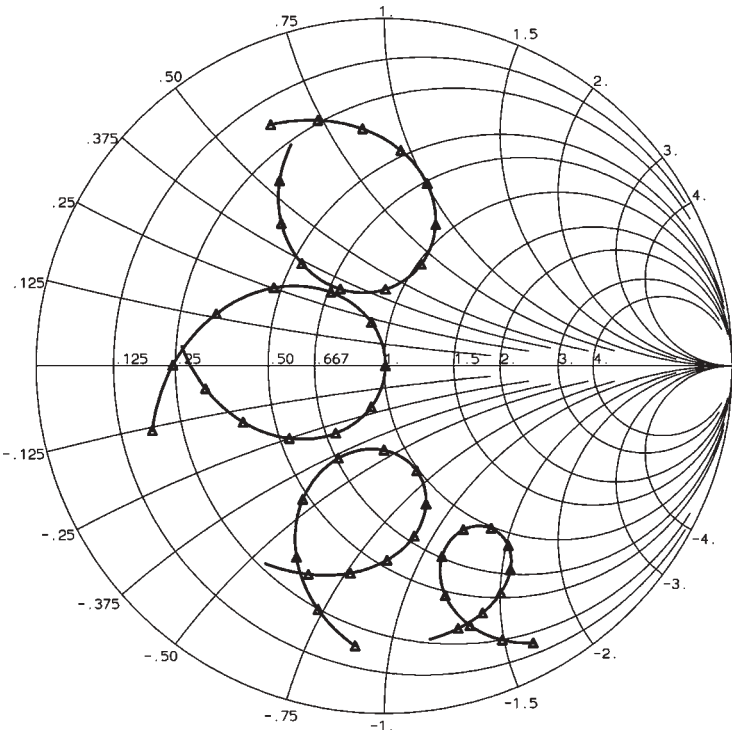

FIGURE 6-18 Effect of varying length of an open-circuited stub in an aperture-fed patch when critically coupled.

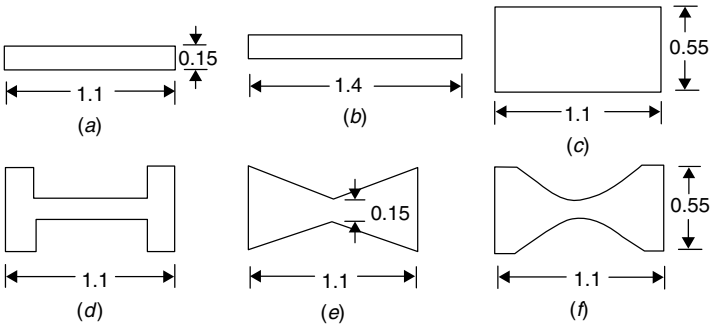

FIGURE 6-19 Aperture shapes to increase coupling and bandwidth. (From [16], Fig. 4-29, © 2003 Artech House, Inc.)

Q decreases and the aperture size grows. This slot, although below a resonant size, increases its radiation and decreases the front-to-back ratio because it radiates equally on both sides. One solution is to enclose the microstrip line in a box to prevent slot radiation on the back side. If we use a high-dielectric-constant substrate for the microstrip line, the coupling through the aperture remains high, but the second ground plane of the microstrip will reduce the coupling. The slot aperture adds a pole to the patch circuit that can be used to broadband the impedance response. To use this pole effectively, we must increase the aperture size until it becomes a significant radiator.

6-4 QUARTER-WAVE PATCH ANTENNA

When operation is in the lowest mode, a virtual short circuit forms through a plane centered between the two radiating edges. We can make an antenna by using half the patch and supplying the short circuit (Figure 6-20). The E-plane pattern broadens to that of a single slot. The resonant length is about a quarter-wavelength in the dielectric of the substrate. We use the effective dielectric constant ε_{eff} of a microstrip line of patch width W and Δ given by Eq. (6-18) to determine the resonant length L of the quarter-wave patch:

$$\frac{L}{2} = \frac{\lambda}{4\sqrt{\varepsilon_{\text{eff}}}} - \Delta \tag{6-26}$$

We can implement the short circuit with a series of pins or etched vias between the ground plane and the patch. These add an inductive component to the transmission-line model of the antenna. The effective shorting plane occurs further along the transmission line. The equivalent extra length Δl is found from the parallel-plate circuit model of a row of evenly spaced pins [17, p. 104]. Given the pin center spacing S, their radius r, and the wavelength in the dielectric $\lambda_d = \lambda_0/\sqrt{\varepsilon_r}$, we compute the patch-length reduction from the equation

$$\Delta l = \frac{S}{2\pi}\left[\ln\frac{S}{2\pi r} - \left(\frac{2\pi r}{S}\right)^2 + 0.601\left(\frac{S}{\lambda_d}\right)^2\right] \tag{6-27}$$

We have only the conductance and susceptance of a single edge that doubles the resonant resistance at the edge as compared with the full patch. It becomes difficult to feed the antenna from microstrip because this raises the quarter-wavelength transformer impedance and requires narrower lines. We can increase the edge width to reduce the edge input resistance, but the antenna is usually fed from underneath. Equation (6-23) gives the approximate feed location measured from the short circuit. The resonant frequency shifts slightly as the feed point moves. During tuning for impedance match, the length of the cavity will have to be adjusted to maintain the desired resonant frequency. Quarter-wave and full-patch antennas have the same Q. A half-patch antenna has half

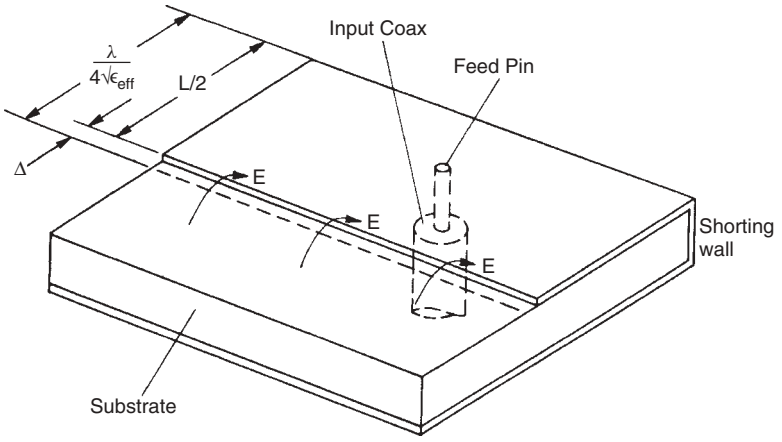

FIGURE 6-20 Quarter-wave patch.

the radiation conductance but only half the stored energy of a full-patch antenna. Its bandwidth is approximately the same as that of the full patch.

Example Design a half-patch antenna at 5 GHz on a 0.8-mm-thick substrate ($\varepsilon_r = 2.21$) with a radiating width of 0.75λ.

The edge width is $0.75(300\,\text{mm})/5 = 45\,\text{mm}$. By using Eq. (6-19), we compute the effective dielectric constant in the cavity: $\varepsilon_{\text{eff}} = 2.16$. Equation (6-18) gives us the cutback for fringing fields: $\Delta = 0.42\,\text{mm}$. The resonant length becomes

$$\frac{L}{2} = \frac{\lambda}{4\sqrt{\varepsilon_{\text{eff}}}} - \Delta = 10.20 - 0.42 = 9.78\,\text{mm}$$

The radiation conductance from the single edge is [Eq. (6-20)]

$$G = \frac{45}{120(60)} = 6.25\,\text{mS} \quad \text{or} \quad R = 160\ \Omega$$

The 50-Ω feed point is found from Eq. (6-23):

$$x = \frac{19.56}{\pi}\sin^{-1}\sqrt{\frac{50}{160}} = 3.69\,\text{mm}$$

where x is the distance from the short.

The short circuit of this antenna is quite critical. The low impedance of the microstrip cavity raises the currents in the short circuit. Without a good low-impedance short, the antenna will detune and have spurious radiation. If the antenna is made from a machined cavity, careful attention must be paid to the junction between the top plate and the cavity to assure good electrical contact.

Figure 6-21 shows the calculated pattern of a quarter-wave patch on a free-space substrate 0.04λ thick on an infinite ground plane. The antenna radiates primarily from the single edge located opposite the short-circuited edge. A vertical probe feeds the

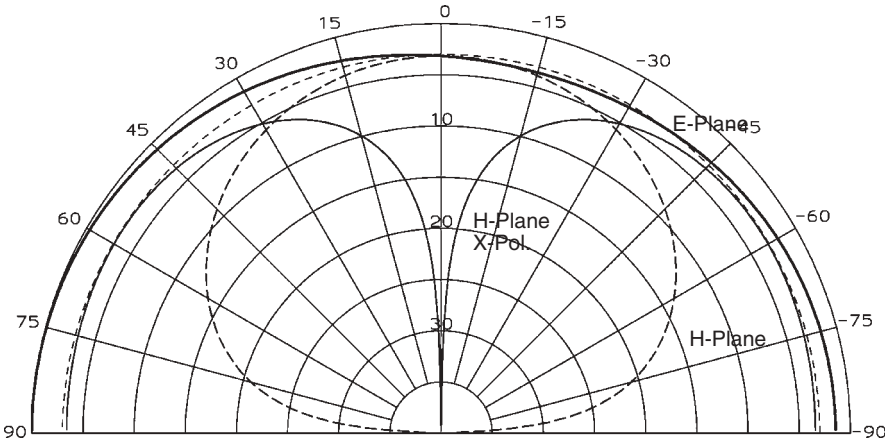

FIGURE 6-21 Pattern of a quarter-wave patch on a free-space substrate.

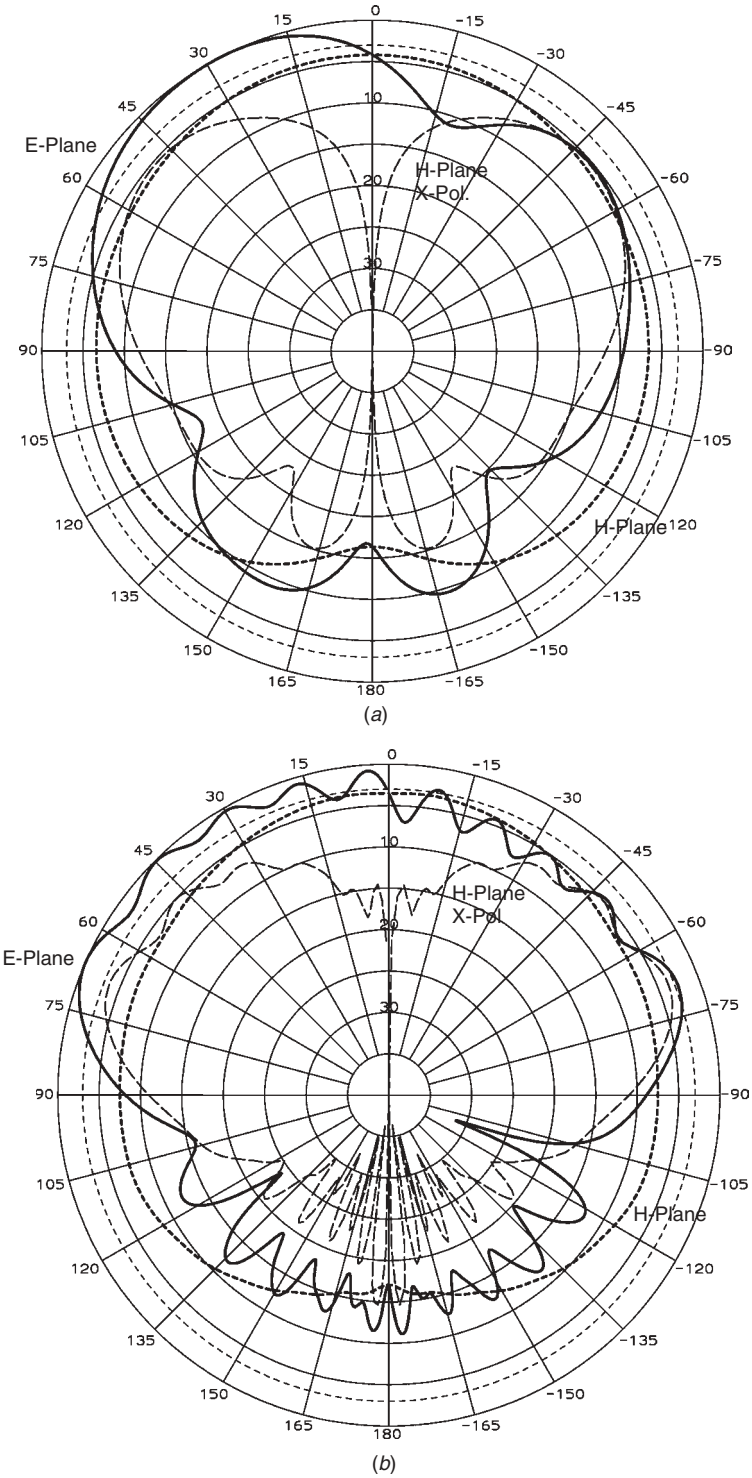

FIGURE 6-22 Pattern of a quarter-wave patch mounted on (*a*) 2λ- and (*b*) 10λ-diameter ground planes.

antenna directly. The E-plane has a broad, nearly constant pattern. Radiation from current on the probe and shorting pins adds to positive angle radiation of the equivalent single slot while subtracting in the opposite direction. The H-plane pattern (dashed curve) retains its null along the ground plane. The light-line curve gives the cross-polarization in the H-plane. The feed probe and shorting pin currents produce a pattern similar to that from a monopole. The model that uses equivalent magnetic currents fails to predict the high radiation from these currents. When the quarter-wave patch is mounted on a finite ground plane, it exhibits behavior similar to that of a monopole. Figure 6-22*a,b* plots the pattern when it is mounted on 2λ- and 10λ-diameter ground planes. These show a monopole-type pattern, where radiation spreads readily behind the ground plane. Currents flowing in the feed pin and shorting wall distort the E-plane and cause asymmetry. The magnetic currents flowing along the side slots no longer cancel as in the square patch and increase cross-polarization.

If we close off the nonradiating edges with metal walls, the walls convert the parallel-plate line into a waveguide and we use the waveguide propagation constant to calculate the quarter-wavelength cavity depth. The slot fields vanish on the ends and establish a sinusoidal slot distribution. We can offset the feed toward both the back wall and the sidewall to reduce the input impedance. The peak voltage (minimum current and peak resistance) occurs at the slot center. Figure 6-23 illustrates the pattern of the waveguide quarter-wave patch on an infinite ground plane. The sidewalls reduce the monopole radiation, and the H-plane cross-polarization is reduced compared to a quarter-wave patch. When mounted on a 2λ-diameter disk, centered on the feed pin, the pattern (Figure 6-24) exhibits lower-level radiation in the backlobe because the monopole pattern has been reduced. The high radiation level at the disk edges still causes considerable edge diffraction in the E-plane.

6-5 CIRCULAR MICROSTRIP PATCH

In some applications, a circular patch fits in the available space better than a rectangular one. In a triangularly spaced array, they maintain a more uniform element

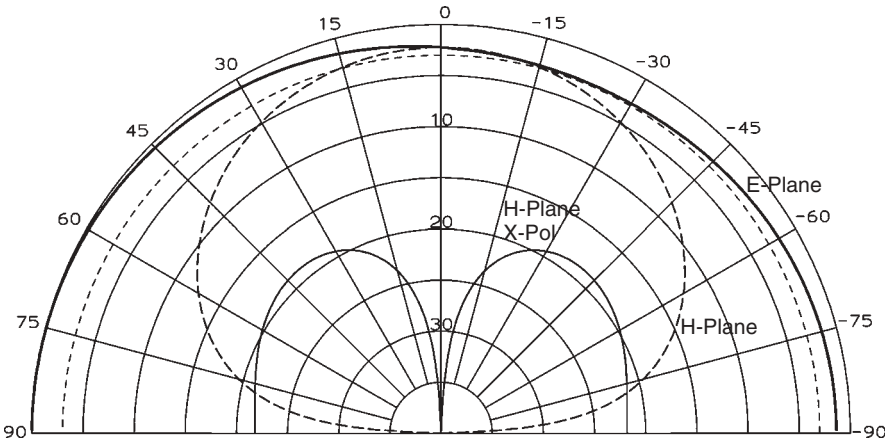

FIGURE 6-23 Pattern of a quarter-wave waveguide patch.

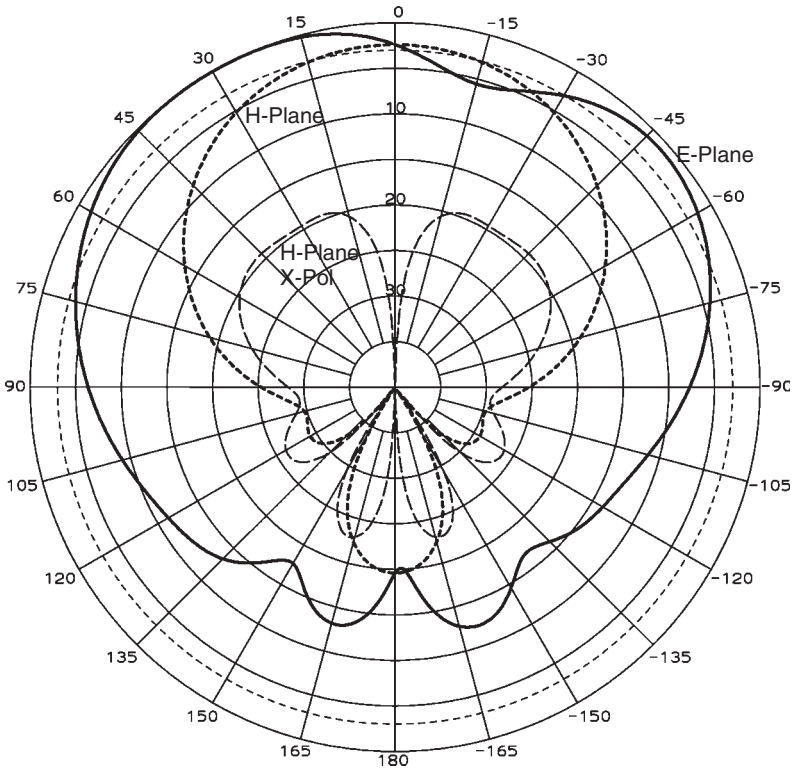

FIGURE 6-24 Quarter-wave waveguide patch mounted on a 2λ-diameter disk.

environment. No suitable transmission-line model presents itself, and the cavity model must determine the resonant frequency and bandwidth. The cutoff frequencies of TE modes of circular waveguides give the resonant frequencies of circular patch antennas. The patch with its magnetic walls and TM modes is the dual of the waveguide. The resonant frequencies are given by

$$f_{np} = \frac{X'_{np} c}{2\pi a_{\text{eff}} \sqrt{\varepsilon_r}} \tag{6-28}$$

where X'_{np} are the zeros of the derivative of the Bessel function $J_n(x)$ of order n, as is true of TE-mode circular waveguides. The term a_{eff} is an effective radius of the patch [18]:

$$a_{\text{eff}} = a\sqrt{1 + \frac{2H}{\pi a \varepsilon_r}\left(\ln\frac{\pi a}{2H} + 1.7726\right)} \tag{6-29}$$

where a is the physical radius and H is the substrate thickness. Using the effective radius gives the resonant frequency within 2.5%.

We combine Eqs. (6-28) and (6-29) to determine radius to give a particular resonant frequency:

$$a_{\text{eff}} = \frac{X'_{np} c}{2\pi f_{np} \sqrt{e_r}} \tag{6-30}$$

Since a and a_{eff} are nearly the same, we can iterate Eq. (6-29) to compute a, the physical radius [19, p. 119]:

$$a = \frac{a_{\text{eff}}}{\sqrt{1 + 2H/\pi a\varepsilon_r \left[\ln(\pi a/2H) + 1.7726\right]}} \tag{6-31}$$

We start by using a_{eff} for a in Eq. (6-31), which converges rapidly. The lowest-order mode, TM_{11}, uses X'_{11} (1.84118) and produces a linearly polarized field similar to a square patch. The TM_{01} mode ($X'_{01} = 3.83171$) produces a monopole-type pattern from a uniform edge fringing field.

Example Design a circular microstrip patch antenna (TM_{11} mode) at 3 GHz on a 1.6-mm substrate that has a dielectric constant of 2.55 (woven Teflon fiberglass).

We calculate the effective radius from Eq. (6-30):

$$a_{\text{eff}} = \frac{1.84118(300 \times 10^9 \text{ mm/s})}{2\pi(3 \times 10^9 \text{ Hz})\sqrt{2.55}} = 18.35 \text{ mm}$$

The physical radius will be slightly less. By using a_{eff} in the denominator of Eq. (6-31), we obtain a physical radius: $a = 17.48$ mm. We can then substitute this back into Eq. (6-31) and obtain $a = 17.45$ mm. Equation (6-31) converges in two iterations to a reasonable tolerance, since another iteration gives the same value. Actually, a single iteration gives the value within 0.2% on a formula accurate to only 2.5%.

The fields of the TM_{11} mode produce a virtual short circuit at the center of the patch. We can reinforce the short circuit with a pin soldered between the patch and ground. The radial line along which the feed is placed determines the direction of the linear polarization. The nonuniform radiation along its edge gives a larger edge impedance than the square patch. Experience shows that the 50-Ω feed point is located from the center at about one-third the radius. Experiments, actual or numerical, will be required to locate the proper point. Use a network analyzer with a Smith chart display to measure the input impedance. If the resonance circle swings around the origin, the impedance is too high (overcoupled). Move the feed toward the center. A scalar return-loss display cannot give you the direction of movement required. Like the rectangular patch, mismatching the impedance at center frequency to about 65Ω increases the bandwidth slightly. Derneryd [20] gives an approximate expression for the radial impedance variation:

$$R_{\text{in}} = R_e \frac{J_1^2(k_\varepsilon \rho)}{J_1^2(k_\varepsilon a)} \tag{6-32}$$

where R_e is the edge resistance, ρ the radial distance, and J_1 the Bessel function of the first kind. k_ε is the propagation constant in the substrate dielectric constant: $k_\varepsilon = k\sqrt{\varepsilon_r}$. Figure 6-25 gives the 2 : 1 VSWR bandwidth of a circular patch on various substrates as a function of the substrate thickness. It has a slightly smaller bandwidth than that of a square patch because it has a smaller volume. The curves on Figure 6-25 include surface-wave radiation (or losses).

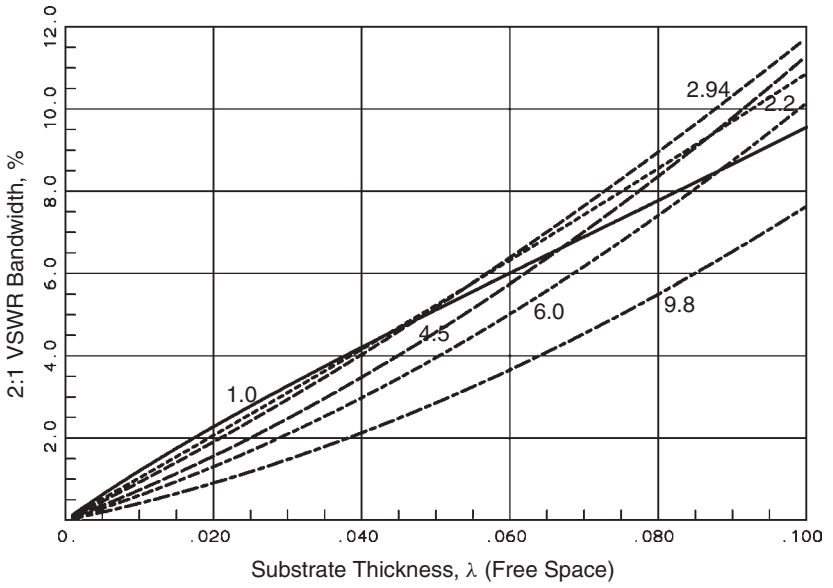

FIGURE 6-25 2 : 1 VSWR bandwidth of circular microstrip patches versus substrate thickness in free-space wavelengths, including surface-wave radiation.

6-6 CIRCULARLY POLARIZED PATCH ANTENNAS

Figure 6-26 show methods of achieving circular polarization with square patches fed with two inputs. The patches are fed by equal signals 90° out of phase. The branchline hybrid (Figure 6-26*a*) consists of four transmission lines connected in a square. The hybrid shown (100-Ω system) produces equal outputs 90° out of phase at center frequency. The two inputs produce patterns with opposite senses of circular polarization. Both the VSWR and axial ratio bandwidths far exceed the singly fed patch bandwidth. Reflections due to the patch mismatch are routed to the opposite input. Patch input reflections, undetected at the input, reduce the efficiency of the antenna by the same amount as the singly fed patch mismatches. The antenna can be fed from below in two places by using a coupled line hybrid, but it suffers from the same efficiency problem.

The cross-fed antenna (Figure 6-26*b*) splits the signal to feed both edges. A quarter-wavelength-longer line provides the extra 90° phase shift to give circular polarization. Shifting the impedance from one input through a quarter-wavelength line before adding the two in shunt cancels some of the reflection from the second line and increases the impedance bandwidth. The impedance bandwidth approximately doubles compared to the singly fed patch. The 6-dB axial ratio bandwidth roughly equals the singly fed square-patch bandwidth. The polarization loss (0.5 dB) of a 6-dB axial ratio equals the 2 : 1 VSWR mismatch loss.

The antennas in Figure 6-27 use asymmetries to perturb the resonance frequencies of two possible modes and achieve circular polarization [21]. The approximately square patches have been divided into two groups: type A, fed along the centerline, and type B, fed along the diagonal. All these antennas radiate RHC. We can understand the operation of these patches from an analysis of the turnstile dipole antenna (Figure 6-28). The orthogonal dipoles could be of equal length and fed from a 90° hybrid to achieve

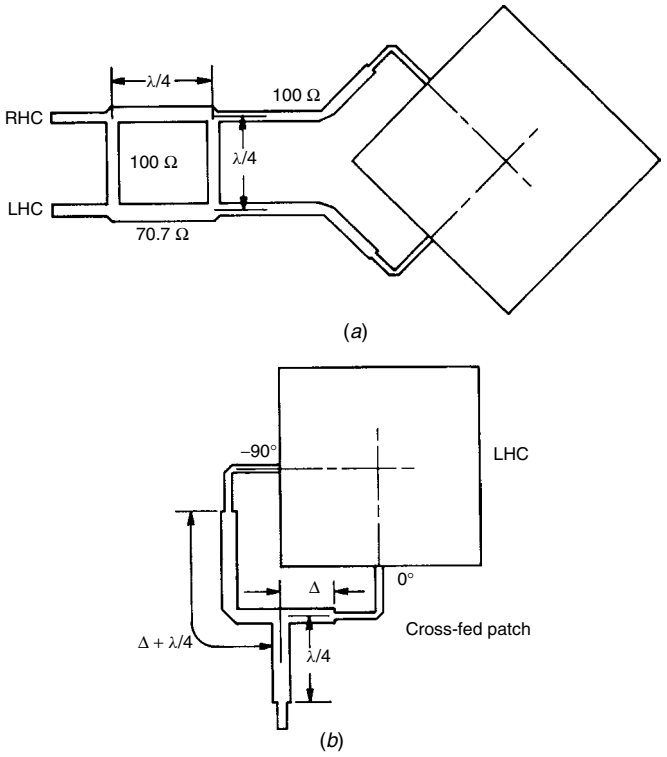

FIGURE 6-26 Dual-fed circularly polarized patch antennas: (*a*) branchline hybrid fed; (*b*) cross-fed patch.

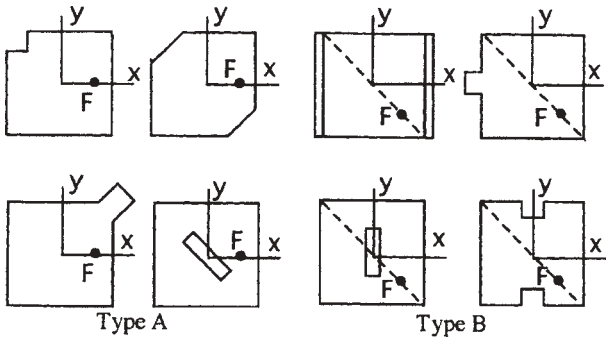

FIGURE 6-27 Classes of perturbed microstrip patches to generate circular polarization from a single feed. (From R. Garg et al., *Microstrip Patch Handbook*, Fig. 8-15, © 1999 Artech House, Inc.)

circular polarization (like the patch in Figure 6-26*a*). Instead, the lengths are changed to shift the phase of each dipole by 45° at resonance. If we lengthen the dipole beyond resonance, the input impedance becomes inductive. The current becomes

$$I = \frac{V}{R_2 + jX_2} = \frac{V(R_2 - jX_2)}{R_2^2 + X_2^2}$$

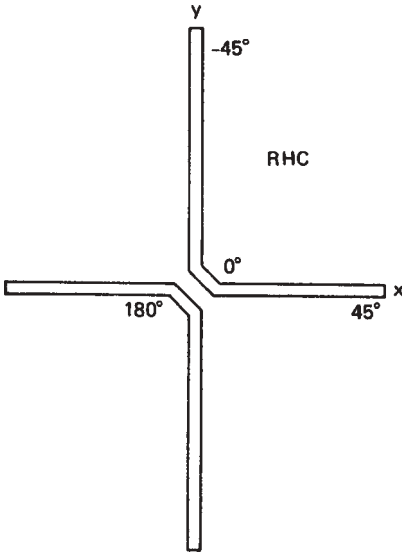

FIGURE 6-28 Turnstile dipole antenna.

The radiated field phase decreases relative to the resonant-length dipole. Shortening the dipole from resonance increases the far-field phase. We adjust the lengths until the phase difference of the radiated fields is 90° and the susceptances from the two dipoles cancel at center frequency. The combination of the two modes produces a Smith chart response with a small loop or kink (see Figure 5-13). The best circular polarization occurs at the frequency of the kink, and the response degrades below and above this frequency. The axial ratio bandwidth is far less than the impedance bandwidth, because the combination of the two modes causes a cancellation of transmission-line reflections from the two modes and increases the impedance bandwidth. The phase required for good circular polarization changes rapidly.

We denote the total change in area ΔS to achieve two resonances for a normal patch area of S and it is proportional to the Q. A type A patch, fed along the square patch axis, requires less area change than a type B patch, fed along the diagonal:

$$\text{type A:} \frac{\Delta S}{S} = \frac{1}{2Q} \qquad \text{type B:} \frac{\Delta S}{S} = \frac{1}{Q} \tag{6-33a,b}$$

We achieve the same effect with a patch by perturbing the lengths of a square patch and feeding both polarizations. An input along the diagonal (type B) feeds all edges in two separate resonances. The ratio of the edge lengths is found in terms of Q by a perturbation technique [4]. We rearrange Eq. (6-33*b*) to derive the ratio of these lengths:

$$\frac{b}{a} = 1 + \frac{1}{Q} \tag{6-34}$$

We calculate resonant frequencies for the two lengths from Eq. (6-34):

$$f_1 = \frac{f_0}{\sqrt{1 + 1/Q}} \qquad f_2 = f_0\sqrt{1 + \frac{1}{Q}} \tag{6-35}$$

Q is related to the VSWR bandwidth by Eq. (6-7). The 3-dB axial ratio bandwidth of the antenna is limited to $35\%/Q$ or 35% of the frequency difference between f_1 and f_2.

Example Compute resonant lengths for a corner-fed patch on a 1.6-mm substrate with $\varepsilon_r = 2.55$ at 3 GHz.

We have $\lambda = 100$ mm and thickness/$\lambda = 0.016$. From Figure 6-7 we read the 2 : 1 VSWR bandwidth: 1.61%. From Eq. (6-7) we calculate Q:

$$Q = \frac{1}{0.0161\sqrt{2}} = 43.9$$

We use Eq. (6-35) to determine the resonant frequencies:

$$f_1 = \frac{3}{\sqrt{1 + 1/43.9}} = 2.966\,\text{GHz}$$

$$f_2 = 3\sqrt{1 + 1/43.9} = 3.034\,\text{GHz}$$

By using the techniques of Section 6-3, we calculate the resonant lengths: $a = 30.27$ mm, $b = 31.01$ mm.

All perturbations by small areas in a circular patch can only be type A feeding. The perturbation equations are related to the circular patch separation constant X'_{11} (1.84118):

$$\text{type A:} \frac{\Delta S}{S} = \frac{1}{X'_{11} Q} \qquad \text{type B:} \frac{\Delta S}{S} = \frac{2}{X'_{11} Q} \tag{6-36}$$

A circular patch perturbed into an elliptical patch radiates circular polarization when fed on a 45° diagonal from the major or minor axis and produces type B feeding. The ratio of major to minor axes is related to Q [4]:

$$\frac{b}{a} = 1 + \frac{1.0887}{Q}$$

with resonant frequencies

$$f_1 = \frac{f_0}{\sqrt{1 + 1.0887/Q}} \quad \text{and} \quad f_2 = f_0\sqrt{1 + \frac{1.0887}{Q}} \tag{6-37}$$

We compute Q by using Eq. (6-7) and read the bandwidths from Figure 6-25 for circular patches. Use the techniques of Section 6-5 to calculate the physical radius of the major and minor axes from the frequencies [Eq. (6-35)].

6-7 COMPACT PATCHES

The desire to produce small patches for cellular telephone handset use has lead to the development of compact designs. The ideal antenna is one whose location the user is unaware of and which is as small as possible. Because most signals arrive at the user

after many bounces and edge diffractions, polarization is arbitrary. We do not need to control the radiation pattern or its polarization carefully and it opens up a range of possibilities. Shorting pins placed close to the feed pin reduce the patch size to about $\frac{1}{8}\lambda$ on a side, but its polarization is poorly controlled. If we can force the current to take a longer path along the resonant-length path, we can shrink the overall size. We etch notches in the patch to make the current wander or use various spiral-wound networks on a flat substrate. Three-dimensional solutions consist of folding a patch by using the vertical direction or some sort of winding around a cylinder. Many variations on these ideas appear in the literature and in collections of these ideas [16,22,23].

Adding a shorting pin closely spaced to the vertical feed pin (Figure 6-29) greatly reduces the resonant frequency of a given-size patch and produces a compact patch [24]. The idea is to make the current flow over a longer path from the feed point to the radiation site; in other words, the transmission line has been folded to make the path longer in the resonant cavity. We use this concept for all compact patches. In this configuration the resonant wavelength is found from the patch perimeter. Given the width W and the length L of the patch on a dielectric substrate ε_r, the resonant wavelength is given by

$$\lambda_0 = 4\sqrt{\varepsilon_r}(L + W) \tag{6-38}$$

which reduces to a square patch $\lambda/8$ on a side. This patch has one-half the length and one-fourth the area of a quarter-wave path, with its short circuit along an entire edge. The circular shorting pin compact patch resonant diameter equals $0.14\lambda_0/\sqrt{\varepsilon_r}$. Making a patch this small produces highly inductive input impedance, which we can see by looking at the Smith chart of a coaxial probe-fed patch (Figure 6-12). The curve sweeps clockwise as the frequency increases. At low frequency (or small size) the patch is highly inductive. Figure 6-12 shows that using thicker substrates to increase bandwidth makes the patch impedance even more inductive. The shorting pin next to the feed pin forms a transmission line with it and adds a capacitive component to the input impedance that counteracts the patch and feed pin inductance. As the shorting pin is moved farther away from the feed pin, the capacitance decreases and the shorting pin becomes an inductive component, as it is in the quarter-wave patch.

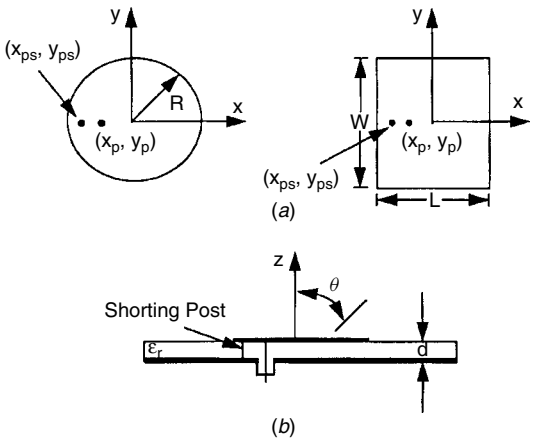

FIGURE 6-29 Compact patch with a shorting pin near the feed. (From [24], Fig. 1, © 1998 IEEE.)

The recommended position of the shorting pin is 80 to 90% of the distance from the center to the outer edge and a diameter of 0.008λ. You will need to iterate the position of the feed probe, usually one-half the diameter of the shorting pin, to achieve an impedance match. Table 6-5 lists the bandwidth achieved versus substrate thickness on foam, $\varepsilon_r = 1.07$ [25, p. 207].

Figure 6-30 gives the calculated pattern of a shorting pin compact patch on 0.034λ free-space substrate. The broad E-plane pattern has 10-dB dip on the broadside matched by the H-plane E_ϕ component. The large current in the shorting pin produces a significant monopole pattern seen in the E_θ radiation in the H-plane. This small antenna is a combination of a top-loaded monopole and a patch. Thinner antennas have a lower pattern dip broadside to the substrate because the monopole is shorter.

The planar inverted F antenna (PIFA) is similar electrically to the shorting pin compact patch. We move the shorting pin to one corner and often make it a small shorting plate. We locate the feed pin close to the small shorting plate to again form a transmission line whose capacitance with the feed pin counteracts the inductive component of the small patch. We use Eq. (6-38) to determine its resonant wavelength. If we rotate the coordinates so that the shorting plate and diagonal lie on the x-axis, we obtain the pattern response of Figure 6-30. Since there is practically no difference between the two antennas, Table 6-5 gives the bandwidth of the PIFA versus thickness [26].

TABLE 6-5 Bandwidth of a Single Shorting Pin Compact Patch

Thickness (λ_0)	Bandwidth, 2 : 1 VSWR (%)	Feed-to-Pin Center Distance (λ_0)
0.01	1.6	0.0071
0.02	2.2	0.0076
0.03	2.7	0.0081
0.04	3.4	0.0085
0.05	4.3	0.0101
0.06	5.7	0.0135

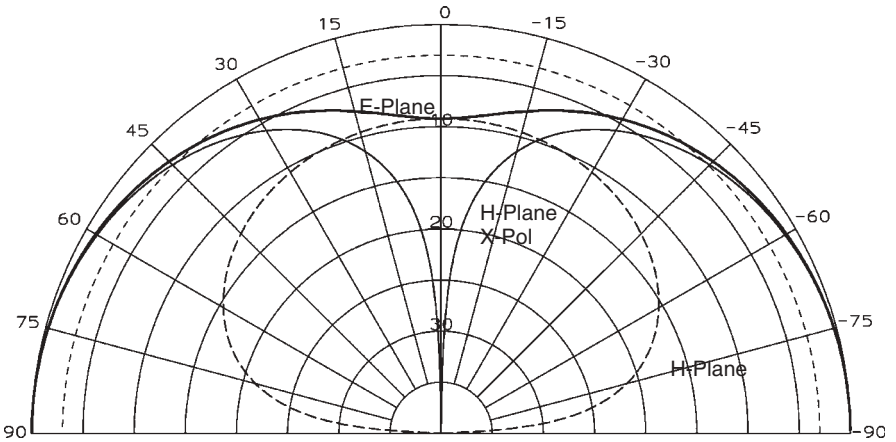

FIGURE 6-30 Pattern of a compact patch.

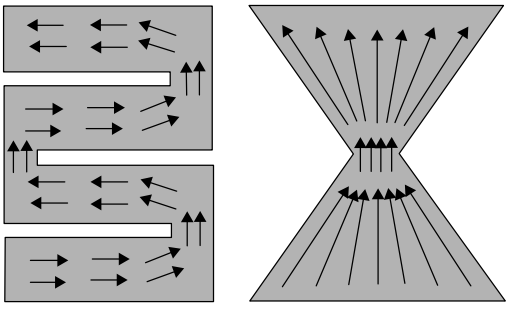

FIGURE 6-31 Reduced-size microstrip patches using meandered current paths. (From [22], Fig. 1-3, © 2002 John Wiley & Sons, Inc.)

Modest size reduction can be obtained by making the currents flow along a longer path along the resonant length. Figure 6-31 shows two planar antennas where slits cut from the width sides and disrupting the resonant-length path cause wandering of the current. The bowtie patch also makes the current path longer. These antennas radiate normal patch patterns with broader beamwidths in the E-plane because the notches bring the radiating edges closer together. The antennas in Figure 6-32 shrink the resonant length by folding the antennas vertically. The total length along the path is approximately $\lambda/2$, but the radiating edges are closer together. A large number of variations using slots have been investigated and offer interesting approaches to both shrink the patch size and produce dual-frequency antennas by using both the patch mode and slot radiation [22].

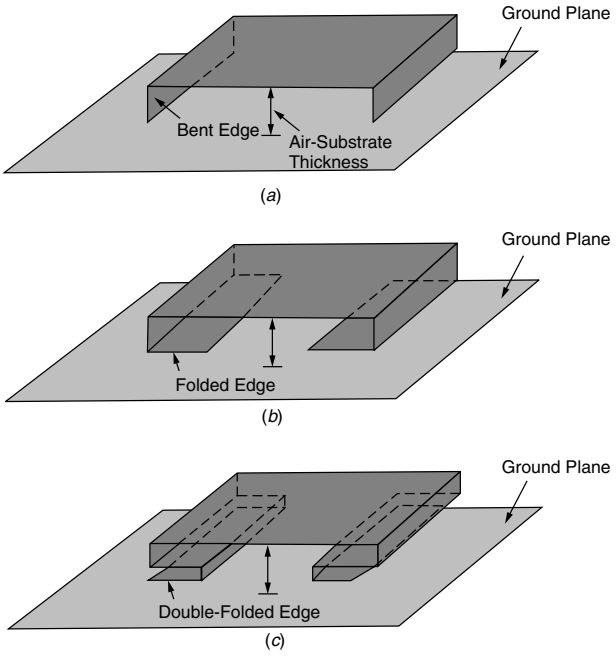

FIGURE 6-32 Folding microstrip patches to reduce size. (From [22], Fig. 1-4, © 2002 John Wiley & Sons, Inc.)

6-8 DIRECTLY FED STACKED PATCHES

Figure 6-7 illustrates the limited impedance bandwidth achievable from a single-resonator microstrip patch. When we increase the substrate thickness to widen the bandwidth, the antenna excites more surface waves (Figure 6-8) difficult to control, and we accept them as losses. In Section 6-3 we discussed the use of external circuit elements to improve the impedance response. These have limited usefulness, although the simple series capacitor input to overcome the inductance of a long feed probe and the inductive nature of the higher-order modes is easily implemented. These external elements add poles to the resonant circuit to increase bandwidth. We can increase the number of poles by adding antenna elements instead. One solution is to couple to additional patches located around the fed patch on the same substrate surface. This increases the antenna size and reduces pattern beamwidths. This solution is difficult to use in an array because the large spacing between elements produces grating lobes. Stacking patches vertically above the driven patch and coupling to them electromagnetically produces the best solution in terms of pattern response. The disadvantage of this approach is the additional fabrication cost. Our discussion of aperture-coupled patches in Section 6-3 points out that large apertures also add resonant poles that can increase the bandwidth. These added resonant elements complicate the design and call for the application of analytical tools instead of a cut-and-try approach.

Although either patch in a two-element stacked patch design can be fed, feeding the lower element produces a design with minimum feed pin inductance. Aperture coupling through the ground plane feeds the lower patch directly as well. If we use an edge feed, we want the input transmission line to be as narrow as possible to reduce radiation by feeding the lower patch. Initially, we consider the probe-fed stacked patch [27]. A coaxial probe feeds directly a lower substrate of thickness d_1 and dielectric constant ε_{r1} through a hole in the ground plane. Figure 6-12 shows that the feed probe adds inductance for a thick substrate and the resonant loop is located on the upper inductive portion of the Smith chart. When we couple the lower patch to an upper patch with thickness d_2 and dielectric constant ε_{r2}, its circuit response becomes more inductive. We need to start with the impedance locus of the lower patch to be capacitive without the upper patch. This can be achieved by using an overcoupled feed. Figure 6-11 illustrates the overcoupled patch whose impedance locus sweeps around the origin of the Smith chart. The inductance of the feed probe rotates these curves clockwise around the center of the chart and the overcoupled response has significant capacitive reactance when it sweeps around the origin. If we matched the lower patch critically, upward movement of the locus due to the coupled patch would reduce the impedance bandwidth. Figure 6-33 illustrates these design steps. Figure 6-33*b* shows that increasing the lower patch thickness leads to a longer feed probe that sweeps across the center from a more inductive portion of the Smith chart. Adding the second patch fails to increase the bandwidth relative to the thinner optimum lower patch. The thickness of the upper patch substrate d_2 controls the tightness of the resonant loop. A greater thickness d_2 produces a tighter loop in the Smith chart response that leads to a lower VSWR over a narrower bandwidth. Remember that we cannot use Eq. (6-7) to determine the bandwidth for different VSWR levels because we now have multiple resonators.

If we use a foam upper substrate, the dielectric constant and thickness of the lower substrate determines the surface-wave efficiency. Waterhouse [27] used a dielectric

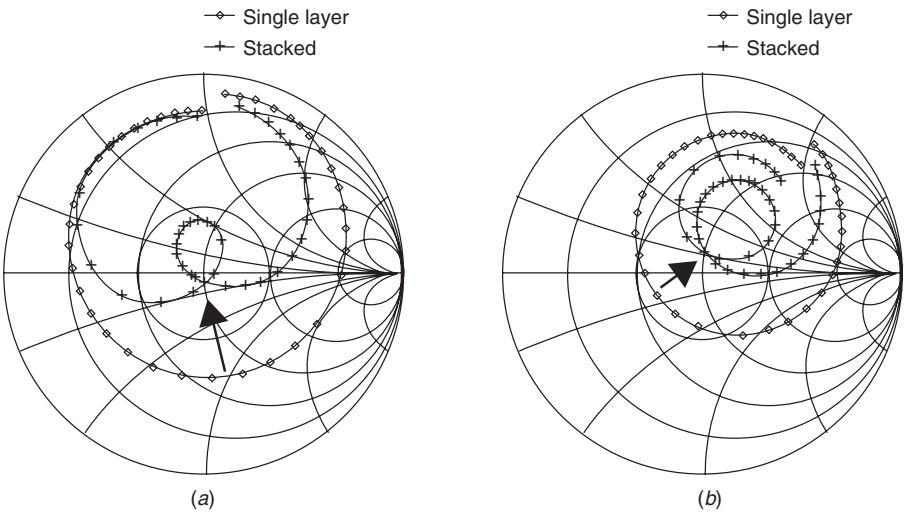

FIGURE 6-33 Effect of coupling to a second patch: (*a*) overcoupled single lower patch response forms resonant loop with the second coupled patch; (*b*) increasing lower patch thickness causes rotation on a Smith chart and lower bandwidth. (From [27], Fig. 3, © 1999 IEEE.)

constant of 2.2 for the lower substrate with a thickness of $0.04\lambda_0$ and a foam upper substrate $0.06\lambda_0$ to achieve optimum bandwidth with acceptable surface-wave losses. The lower patch was overcoupled so that it swept through the 250-Ω resistance point at resonance. Since the impedance locus sweeps clockwise on the Smith chart as frequency increases, this resonant point should be slightly below the lower end of the desired frequency band. We adjust the second substrate thickness to move the resonant loop on the Smith chart in the vertical direction. As we increase the size of the upper patch, the loop moves around an arc in the clockwise direction, which we use to center the impedance response on the Smith chart for optimum bandwidth. This method produces impedance bandwidths of around 25%. The pattern bandwidth exceeds this bandwidth and we expect little change in pattern over this frequency range.

Another successful stacked patch fed from a coaxial probe is the *hi-lo configuration*, in which a high dielectric substrate ($\varepsilon_{r1} = 10.4$) is used for the lower substrate and a foam ($\varepsilon_{r2} = 1.07$) for the upper substrate [25, pp. 178–182]. The upper patch captures the surface wave of the lower patch and greatly improves the overall efficiency by radiating this power in a space wave. Although the two patches have different sizes, the coupling remains sufficient to produce a broadband antenna with impedance bandwidths approaching 30%. In this design the lower patch is designed for the high dielectric of the lower substrate with little consideration for the upper patch except for making it a little overcoupled. The upper patch can be designed using the substrate thickness and dielectric constant assuming that the high dielectric substrate acts as the ground plane. When we mount the upper patch over the smaller lower patch, small adjustments must be made to the dimensions to achieve a 50-Ω impedance match. The example given used a lower substrate thickness of $0.032\lambda_0$ with $\varepsilon_{r1} = 10.4$, and by Figure 6-8 would have −1.3-dB surface-wave loss. Locating the second patch on a $0.067\lambda_0$-thick foam substrate directly over the first patch reduced the surface-wave loss to better than −0.7 dB over the entire band.

6-9 APERTURE-COUPLED STACKED PATCHES

The discussion on aperture feeding of a patch in Section 6-3 stated that we can utilize the aperture as another resonator to broadband the antenna. Figure 6-34 shows the stacked patch antenna fed from an aperture. In this implementation we make the coupling slot long enough to be one of the resonators, which increases the number of resonators to three: the aperture, the lower patch, and the upper patch. We must use element spacing to control coupling because frequencies control resonator sizes. By careful control of parameters two loops will form in the Smith chart response of impedance and be made to wrap tightly around the center of the chart [28] as shown in Figure 6-35*b*. We form these loops by coupling resonators. Undercoupling produces small tight loops; overcoupling produces large loops.

Figure 6-35 illustrates the effect of aperture size. The left Smith chart shows undercoupling between the aperture and the lower patch by the small left loop. We increase the coupling by increasing the aperture slot length (Figure 6-35*b*) or by increasing the

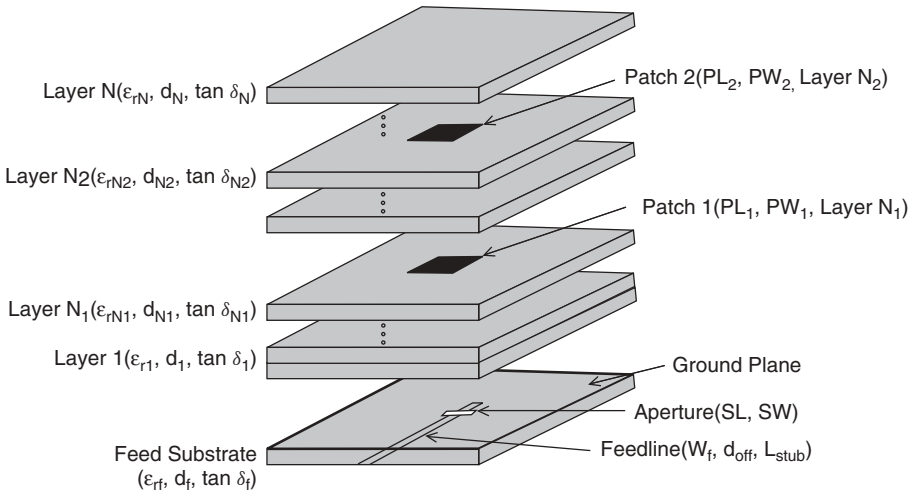

FIGURE 6-34 Construction of a resonant aperture coupled dual patch in exploded view. (From [28], Fig. 1, © 1998 IEEE.)

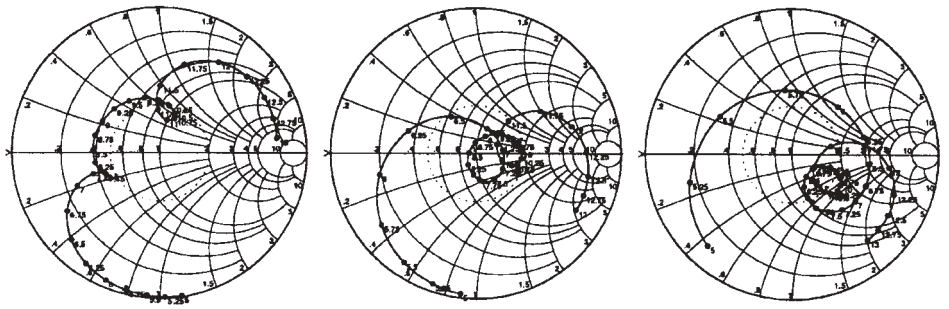

FIGURE 6-35 Effect on increasing slot length, SL, of apertures in stacked dual patches: (*a*) SL = 8 mm; (*b*) SL = 10 mm; (*c*) SL = 12 mm. (From [28], Fig. 4, © 1998 IEEE.)

lower patch size or reducing the lower patch thickness. The best results have been obtained by having the lower-frequency (left) loop determined by the lower patch and aperture. Overcoupling the aperture to the lower patch produces the impedance locus of Figure 6-35*c*. We control the upper loop size by varying the upper patch size, the relative size between the two patches, and the upper substrate thickness. The lower patch size is a critical parameter because it affects the coupling and size of both loops while shifting their center frequencies. For fixed sizes of the other two resonators, decreasing the lower patch size decreases the coupling to the aperture while increasing the coupling to the upper patch. Increasing aperture size increases coupling to the aperture and decreases coupling to the upper patch. By remembering that overcoupling produces larger Smith chart loops, we determine in which direction to change parameters by observing changes in analytical results on the Smith chart to produce optimum designs.

Because the slot aperture is one of the three resonators, we cannot vary its length to determine coupling to the lower patch. The overcoupled large slot produces high resistance at the microstrip input. We can lower this impedance by offset feeding the slot or by using a wide transmission line. A single offset line will unbalance the fields in the slot and lead to unbalanced excitation of the patches. This unbalanced excitation on the patches increases cross-polarization. The dual balanced offset feeding shown in Figure 6-36, where we join the two lines in a reactive power divider, both lowers the resistance and balances the patch excitation.

A design using rectangular patches for a single linear polarization achieved a 67% 2 : 1 VSWR bandwidth [28]. The only significant problem with the design is the poor front-to-back ratio, which is reduced to 6 dB at the upper frequencies as the aperture radiation increases. Placing a reflector patch below the microstrip feed line, it can be sized to reduce the F/B ratio by forming a Yagi–Uda antenna with the stacked patch [29]. Figure 6-37 illustrates an exploded view of a dual polarized aperture stacked patch. The potential bandwidth shrinks because we lose width as a parameter with square patches to optimize impedance. The key element of this design is the feed crossed slot [30]. The crossed-slot feeding aperture is located on a ground plane shared by microstrip networks located below and above the aperture. Each network consists of a reactive power divider to raise the impedance of the feed lines and allow offset feeding of the slot for each polarization. The balanced feed reduces cross-polarization and cross coupling between the two ports that would occur in both the crossed slot

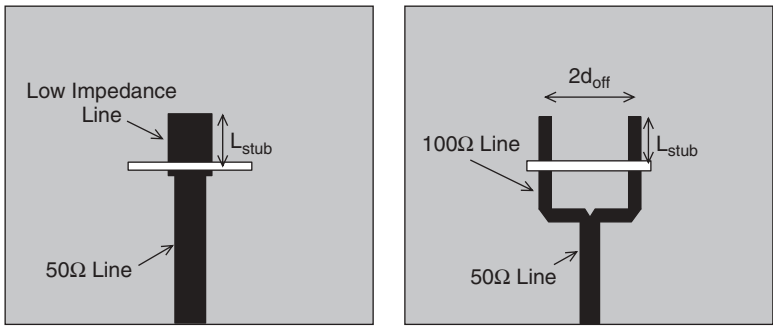

FIGURE 6-36 Impedance matching for resonant aperture dual stacked patches: (*a*) wide transmission line; (*b*) dual offset feed. (From [28], Fig. 3, © 1998 IEEE.)

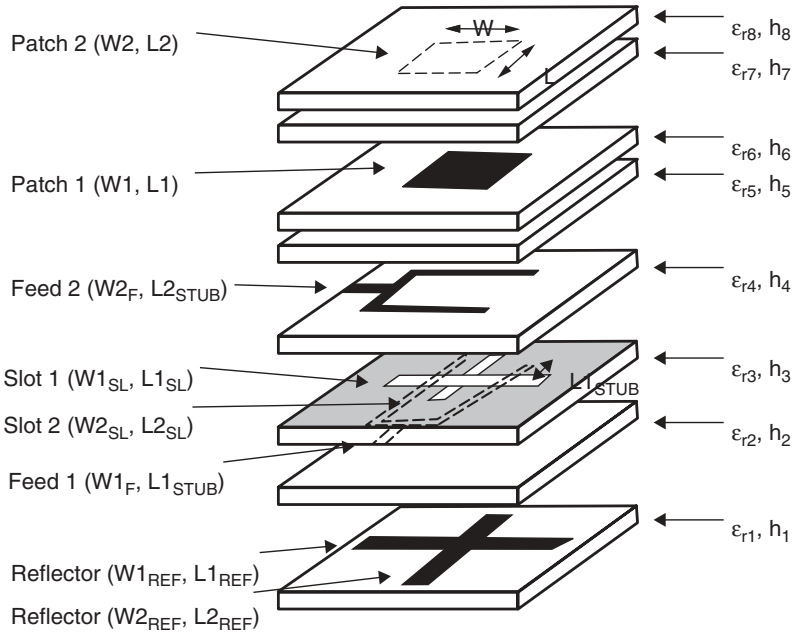

FIGURE 6-37 Exploded view of construction of a dual polarized aperture-fed stacked patch utilizing a crossed strip reflector. (From [8], Fig. 3.6.22, © 2003 Kluwer Academic Publishers.)

and the patch elements. This shows that the slot that couples to a patch resonator can be fed by a microstrip line located either below or above the slot. The ground plane between the two networks for each polarization eliminates direct coupling between the microstrip networks and symmetrical feeding reduces coupling in the slot.

Because we use long slots to feed the lower microstrip patch in an overcoupled excitation, direct coupling of the upper microstrip to the lower patch is minimal in comparison. We use thin substrates of moderate dielectric constant ($\varepsilon_r = 2.2$) to support the etched patches and foam layers between to separate the patches to increase bandwidth and control coupling. Figure 6-37 shows a crossed dipole used as a reflector element below the microstrip feed lines to reflect direct radiation from the crossed slot that reduces the F/B ratio.

6-10 PATCH ANTENNA FEED NETWORKS

Patch antenna arrays may be fed from below (Figure 6-9) by using a stripline distribution network. The connections between the boards greatly complicate the assembly. A connection made vertically from the center strip of a stripline unbalances the fields and induces parallel-plate modes. Shorting pins between the ground planes suppress this mode. It is far easier to etch the feed network on the microstrip and use either edge feeds or aperture feeds with the network located below the patch layer. Feed networks radiate very little in comparison with the patches when etched on the same substrate because radiation from fringing fields on the two sides of the microstrip lines cancel each other except at discontinuities (corners and steps).

Consider the equally fed array (Figure 6-38). Equal amplitude and phase feeding generates virtual magnetic walls between the patches as shown. We can join the edges

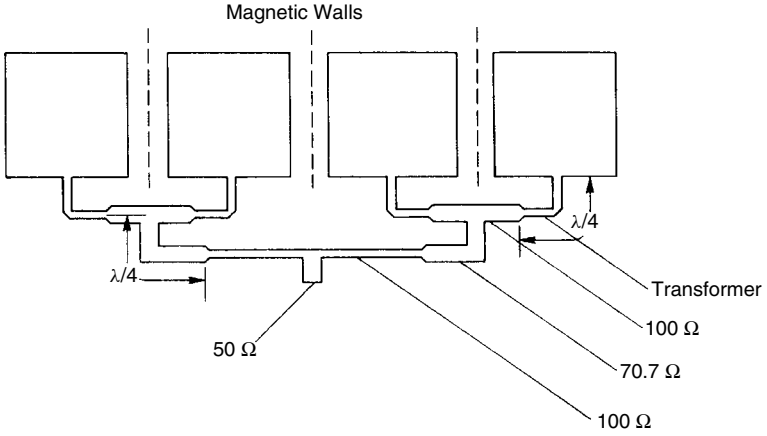

FIGURE 6-38 Equally fed microstrip patch array.

between the patches without effect, since the midpoint remains a virtual open circuit and the separate patches join into a continuous strip. The feeds must be spaced close enough together to prevent grating lobes and to provide uniform amplitude along the edges. These antennas can be wrapped around missiles to provide omnidirectional coverage about the roll axis. To eliminate pattern ripple, feeds must be spaced about every 0.75λ in a circular array. The resistance at each feed at resonance will be the combination of the radiation conductances from the portions of the edges between the magnetic walls.

Figure 6-38 illustrates an equally fed four-element array. Starting from the patch, a quarter-wavelength transformer reduces the roughly 200-Ω impedance to 100Ω. Two 100-Ω lines join in shunt to 50Ω at their juncture. A 70.7-Ω quarter-wavelength line transforms the 50Ω back to 100Ω. We continue this sequence for any 2^N-array for reactive power dividers at each junction. Equal path lengths from the input excite them with equal phases. Arrays with the number of elements different from 2^N-are possible, but they require more difficult feed networks. A 100-Ω system was picked because 50-Ω lines on low-dielectric-constant substrates are quite wide.

The reactive power divider (Figure 6-38) has more bandwidth than the patch while it is matched at the input but not at its outputs. The network can be analyzed by using even and odd modes and shows that the output return loss is 6 dB, and it provides only 6 dB of isolation between outputs. The power reflected from a damaged antenna distributes to the other elements of the array and produces an effect greater than that of just a missing element. Making power dividers with isolation resistors reduces this problem, but we cannot justify the added difficulty of mounting resistors when both good etchings and low probability of damage make them unnecessary.

We must be wary of coupling between different parts of the feed network. We want to pack the feed network into the smallest area, but coupled signals between the lines produce unexpected anomalies. Distinguishing direct radiation from the feed and coupling redistribution is difficult. Although couplings are predictable, they appear as random errors when we cannot perform a full analysis. Unfortunately, the coupling between microstrip lines falls off quite slowly. Table 6-6 lists the coupling and peak errors for 100-Ω lines; those of 50-Ω lines are very similar. We read the amplitude and phase errors from Scales 1-8 and 1-9.

TABLE 6-6 Peak Feed Errors Due to Microstrip Coupling for 100-Ω Lines ($\varepsilon_r = 2.4$)

Spacing/Substrate Thickness	Coupling (dB)	Amplitude Error (dB)	Phase Error (deg)
1.0	16	1.5	9.0
2.0	23	0.7	4.0
3.0	28	0.4	2.3
4.0	32	0.22	1.5
5.0	35	0.12	1.0

6-11 SERIES-FED ARRAY

If we reduce the width of the patch, the radiation conductance is insufficient to match the input. We can use the microstrip patch as a transmission line and connect a line opposite the feed to lead to other patches (Figure 6-39). If we space the patches by half-wavelengths, the impedances of the patches will add in phase at the input, because it rotates once around the Smith chart in $\lambda/2$. The characteristic impedance of the connecting lines has no effect at center frequency. The junction of the transmission-line feeder and the patch introduces excess phase shift. In arrays of a few elements, the extra phase shift can be ignored, but arrays with a large number of elements, or when we design for critical amplitude taper, must account for δ. Of course, traveling-wave or resonant arrays can be designed. The frequency dispersion of the traveling-wave array can be used to frequency-scan the beam.

Various experimental methods have been devised to measure the parameters of the series array. Metzler [31] performed experiments on uniform-width element arrays to determine the radiation conductance and excess phase shift. Measuring the transmission loss through the array as a network with input and output connectors determines the radiation conductance of the patches. An empirical equation was obtained:

$$G = 0.0162\left(\frac{W}{\lambda_0}\right)^{1.757} \qquad 0.033 \le \frac{W}{\lambda} \le 0.254 \tag{6-39}$$

where G is the total radiation conductance of each patch, with half from each edge. Measurement of the beam direction of the uniform traveling-wave array determines the excess phase shift in each patch.

Jones et al. [32] model the patch (Figure 6-39) with extensions Δ due to the fringing fields as a transmission line: $L + 2\Delta$ long. The other excess phase shift, due to the step, is modeled as extensions to the input lines (δ). Jones et al. perform measurements on single elements to establish these lengths. Δ is found from the resonant frequency of the patch: $L + 2\Delta = \lambda/2\sqrt{\varepsilon_{\text{eff}}}$, where ε_{eff} is given by Eq. (6-19). When the transmission-line phase is measured through the patch at resonance, the excess phase beyond π is equated to a phase shift length in the narrow feeder lines:

$$2\delta = \frac{\lambda_N}{2\pi}\phi_{\text{excess}}$$

where λ_N is the wavelength in the narrow line.

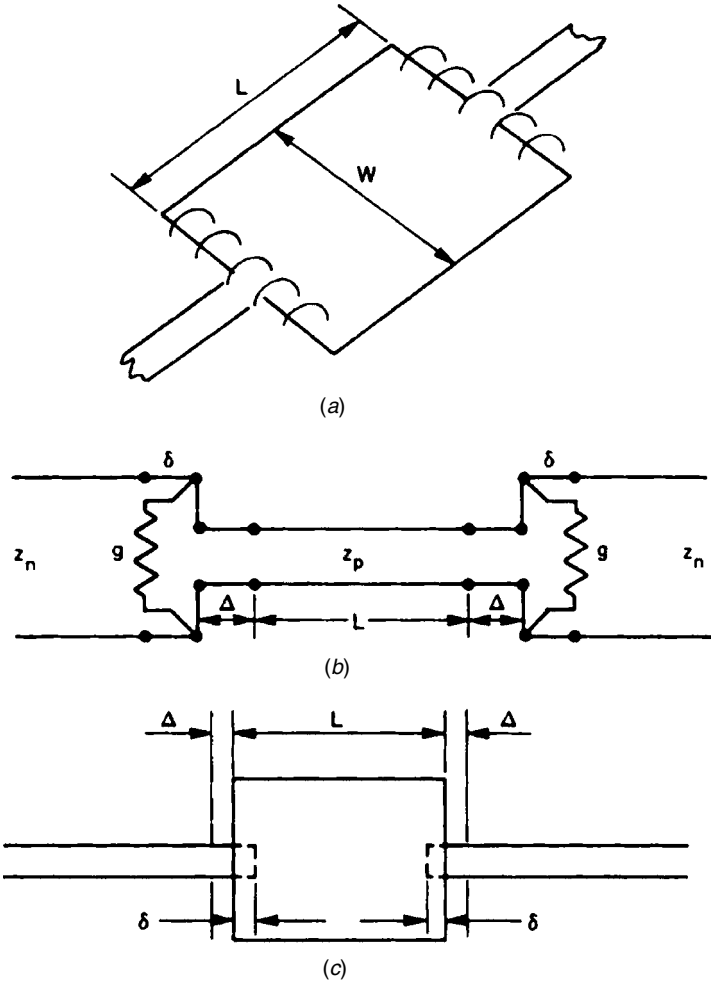

FIGURE 6-39 Series-fed patch and its equivalent circuit. (From [32], Fig. 2, © 1982 IEEE.)

When designing the array, we vary the widths of the patches to achieve the desired amplitude taper. The voltage distribution at each patch is given by $V\sqrt{g}$, where g is the patch conductance. Standing-wave (resonant) arrays require that the sum of the conductances be equal to the input conductance desired. We have some latitude when we feed the array through a quarter-wavelength transformer. The nonresonant array requires a matched load on the end to prevent standing waves. We must pick the ratio of the power dissipated to the radiated power that gives us an extra parameter with which to optimize the design. We control the beam direction by spacing the elements to achieve the phase shift required.

6-12 MICROSTRIP DIPOLE [33]

As the width W of a patch narrows, the input impedance increases. When the width approaches that of a microstrip feed line, either the patch fails to be a resonator or the

feed line becomes very narrow in trying to transform the impedance. The microstrip dipole solves these problems by having a coupled line feeder. The dipole is a half-wavelength strip whose width equals that of a microstrip feed line. A line etched on a substrate below feeds the dipole by coupling into the strip (Figure 6-40*a*). The equivalent circuit (Figure 6-40*b*) transforms the high impedance of the dipole through the unequal coupled lines. By varying the coupling, we can change the input impedance at resonance. Best results occur for quarter-wavelength overlap where the equivalent stubs (Figure 6-40*b*) do not contribute reactance. We vary the coupling by changing the thickness of the substrate between the strips or by offsetting the lower strip.

The dipole radiates as a narrow patch and not as a dipole. No pattern nulls appear along the axis of the strip, but they occur more strongly in the direction of the equivalent magnetic currents of the edges. The H-plane pattern becomes quite broad for the narrow strip width. The feed distribution circuit is etched on the substrate below the dipoles. With the feed circuit on a separate level, we have greater freedom in the feed network design to excite desired distributions. Also, because the dipoles are small, we can use density tapering of the dipoles to that end. Proper design requires measurement [34]

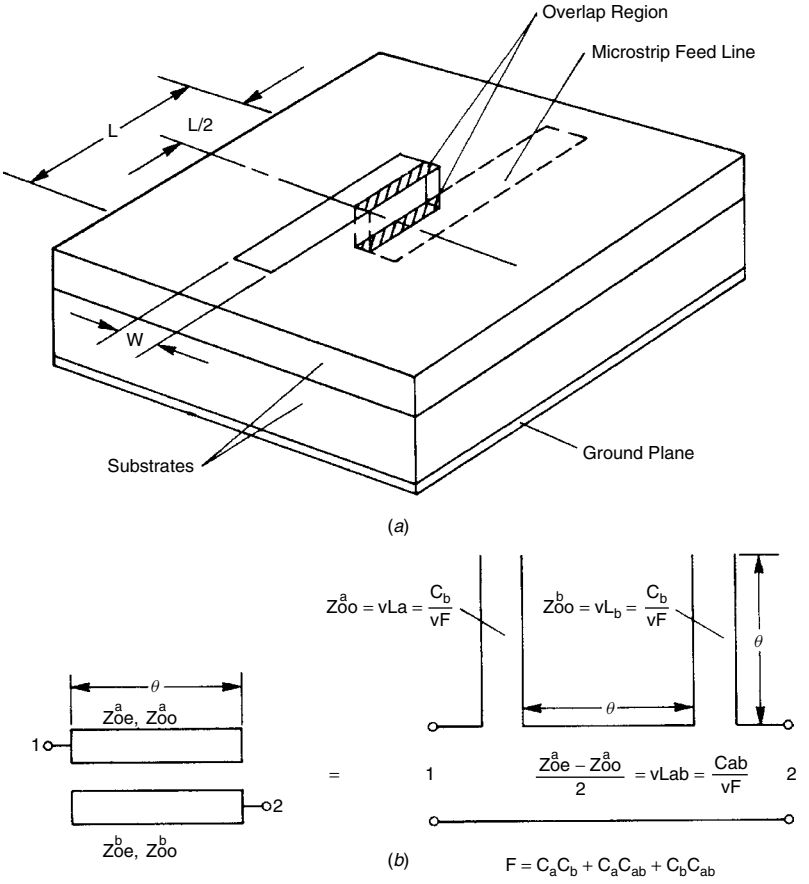

FIGURE 6-40 (*a*) Microstrip dipole; (*b*) equivalent circuit. [(*b*) From G. L. Matthaei et al., *Microwave Filters, Impedance Matching Networks, and Coupling Structures,* © 1980 Artech House, Inc.]

to obtain the desired effect, since mutual coupling will change the distribution by changing the active impedance of each dipole. The feed network must compensate for the coupling.

6-13 MICROSTRIP FRANKLIN ARRAY [35]

An electrically long line with a standing wave on it fails to radiate on broadside because the many cycles cancel each other. We obtain a pattern with many nulls and lobes. By folding the lines with out-of-phase standing-wave currents close together, we can prevent their radiation. The other portions are free to radiate (Figure 6-41*a*). The Franklin array consists of straight sections $\lambda/2$ long connected by $\lambda/4$ shorted stubs. The standing-wave currents on the straight portions add in phase.

We can construct a microstrip version (Figure 6-41*b*). Half-wavelength lines act as radiators (patches). We connect them with half-wavelength lines folded into stubs so that the counteracting standing-wave currents do not radiate. The straight lines are narrow patches. The total radiation conductance of each strip is

$$G = \frac{1}{45}\left(\frac{W}{\lambda}\right)^2 \tag{6-40}$$

for narrow strip widths W, where λ is the free-space wavelength. Using lines for the stubs whose impedance is twice the radiating strip impedance reduces unwanted internal reflections. The two stubs add in shunt. Since the antenna is quite narrowband and the length of the lines between patches is a half-wavelength long, the impedance of these connecting arms has a secondary effect.

Example Design an eight-wavelength array at 10 GHz. There are 16 patches in the array.

The radiation conductances add for elements spaced at $\lambda/2$ intervals. For a 100-Ω input, each patch supplies a conductance 0.01/16. We solve Eq. (6-40) for the width:

$$W = \lambda\sqrt{\frac{0.01(45)}{16}} = 0.168\lambda$$

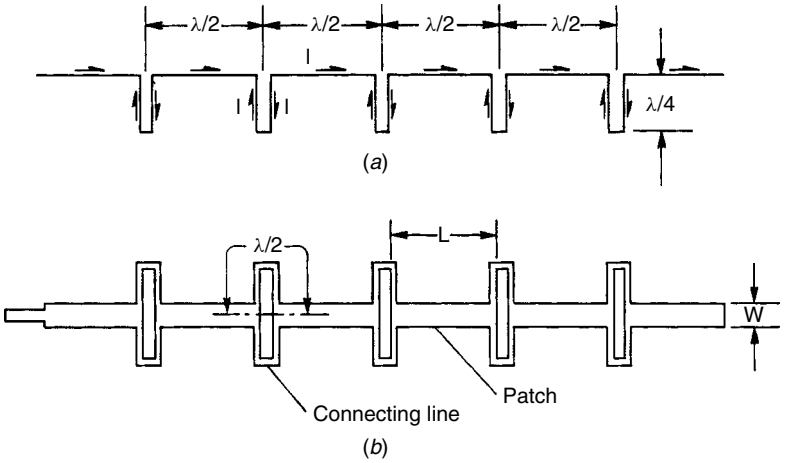

FIGURE 6-41 (*a*) Dipole and (*b*) microstrip Franklin arrays.

If we use Eq. (6-39) from the series patch, we obtain $W = 0.157\lambda$, within the range of the empirical formula. For 10 GHz, $W = 4.71$ mm. On an 0.8-mm substrate ($\varepsilon_r = 2.21$), $W/H = 5.89$ and the impedance of the strip radiator $Z_0 = 44.01\ \Omega$. We need to find the effective dielectric constant of the strip to determine the patch length and impedance. From Eq. (6-19), $\varepsilon_r = 1.97$.

We calculate the cutback from each end by using Eq. (6-18); $\Delta = 0.40$ mm. Each radiating strip is

$$L = \frac{300 \times 10^9}{10^{10}(2)\sqrt{1.97}} - 2(0.40) = 9.88 \text{ mm}$$

The radiating-strip impedance is $Z_0/\sqrt{\varepsilon_{\text{eff}}} = 31.3\ \Omega$. We need 62.6-Ω connecting lines in the stubs to achieve the broadest bandwidth. With so few radiators, we could use 100-Ω connecting arms with little change in bandwidth and have more reasonable connecting arm widths: 0.71 mm.

The example shows that the microstrip Franklin array works best for high frequencies or long arrays. The elements are narrow, and the interconnecting arms are thin.

6-14 MICROSTRIP ANTENNA MECHANICAL PROPERTIES

A microstrip patch antenna has very desirable mechanical properties. It can withstand tremendous shock and vibration. Because the antenna is on a solid substrate, the patch cannot flex, and small changes in the substrate thickness have only a minor effect on the resonant frequency. The commonly used soft substrate (Teflon and fiberglass) has a good damped resilience. Microstrip patch antennas have been used to telemeter data from artillery shells and high-velocity rockets, which have high shock and vibration levels. The repeatability of the dimensions of the patches depends only on the etcher's art. Complicated shapes and feed networks are produced as cheaply as simple ones.

The antennas can withstand exposure to high temperatures when covered by a radome made of the same soft dielectric as the substrate. The cover protects the metal patches but has only a minor effect on the resonant frequency [36]. High temperatures on the surface of the radome or ablation fail to change the resonance significantly because the radome itself has only a minor effect. Variation in the dielectric constant of the substrate from lot to lot causes problems with repeatability. The narrowband antennas require measurement of the dielectric constant of each lot, and sometimes of each sheet, to get the center frequency desired. A series of etching masks can be made to cover the expected range. The antennas can be tuned with inductive shorting pins or capacitive screws, but tuning is prohibitive when the number of elements in an array is large. Careful quality control of the dielectric constant is the answer. Close monitoring of the etching process may also be needed to prevent excessive undercutting.

Temperature variations can be a problem with thin substrates when the bandwidth is narrow. The patch and substrate size grow when the temperature rises, but they are overshadowed by the change in dielectric constant of soft substrates. Instead of decreasing the resonant frequency because of the increased patch size, a lowered dielectric constant raises the center frequency.

Whenever we need more bandwidth than a microstrip patch can provide, we must turn to cavity antennas. We increase the antenna volume by penetrating the vehicle for the cavity, but we gain a design parameter.

REFERENCES

1. R. F. Harrington, Effects of antenna size on gain, bandwidth, and efficiency, *Journal of Research, NBS, D, Radio Propagation*, vol. 64D, January–February 1960, pp. 1–12.
2. R. C. Hansen, Fundamental limitations in antennas, *Proceedings of IEEE*, vol. 69, no. 2, February 1981, pp. 169–173.
3. Y. T. Lo et al., Study of microstrip antenna elements, arrays, feeds, losses, and applications, *Final Report, RADC-TR-81-98*, Rome Air Development Center, Rome, NY, June 1981.
4. K. R. Carver and E. L. Coffey, Theoretical investigation of the microstrip antenna, *Technical Report PT-00929*, Physical Science Laboratory, New Mexico State University, Las Cruces, NM, January 1979.
5. D. R. Jackson and N. G. Alexopoulas, Simple approximate formulas for input resistance, bandwidth, and efficiency of a resonant rectangular patch, *IEEE Transactions on Antennas and Propagation*, vol. 39, no. 3, March 1991, pp. 407–410.
6. R. F. Harrington, *Time-Harmonic Electromagnetic Fields*, McGraw-Hill, New York, 1961.
7. D. M. Pozar, Rigorous closed-form expressions for the surface wave loss of printed antennas, *Electronics Letters*, vol. 26, no. 13, June 21, 1990, pp. 954–956.
8. R. B. Waterhouse, ed., *Microstrip Patch Antennas, A Designer's Guide*, Kluwer Academic, Boston, 2003.
9. R. E. Munson, Conformal microstrip antennas and microstrip phased arrays, *IEEE Transactions on Antennas and Propagation*, vol. AP-22, no. 1, January 1974, pp. 74–78.
10. E. O. Hammerstad, Equations for microstrip circuit design, *Proceedings of the 5th European Micro-strip Conference*, Hamburg, Germany, September 1975, pp. 268–272.
11. M. V. Schneider, Microstrip lines for microwave integrated circuits, *Bell System Technical Journal*, vol. 48, May–June 1969, pp. 1421–1444.
12. D. A. Paschen, Practical examples of integral broadband matching of microstrip antenna elements, *Proceedings of the 1986 Antenna Applications Symposium*, Monticello, IL.
13. T. Samaras, A. Kouloglou, and J. N. Sahalos, A note on impedance variation of a rectangular microstrip patch antenna with feed position, *IEEE Antennas and Propagation Magazine*, vol. 46, no. 2, April 2004.
14. D. M. Pozar, Microstrip antenna aperture-coupled to a microstrip-line, *Electronics Letters*, vol. 21, no. 2, January 1985, pp. 49–50.
15. P. L. Sullivan and D. H. Schaubert, Analysis of an aperture coupled microstrip antenna, *IEEE Transactions on Antennas and Propagation*, vol. AP-34, no. 8, August 1986, pp. 977–984.
16. G. Kumar and K. P. Ray, *Broadband Microstrip Antennas*, Artech House, Boston, 2003.
17. J. R. James, P. S. Hall, and C. Wood, *Microstrip Antennas: Theory and Design*, Peter Peregrinus, London, 1981.
18. L. C. Shen et al., Resonant frequency of a circular disk, printed circuit antenna, *IEEE Transactions on Antennas and Propagation*, vol. AP-25, no. 4, July 1977, pp. 595–596.
19. I. J. Bahl and P. Bhartia, *Microstrip Antennas*, Artech House, Dedham, MA, 1980.
20. A. G. Derneryd, Analysis of the microstrip disk antenna element, *IEEE Transactions on Antennas and Propagation*, vol. AP-27, no. 5, September 1979, pp. 660–664.
21. J. L. Kerr, Microstrip antenna developments, *Proceedings of the Workshop on Printed Circuit Antennas*, New Mexico State University, Las Cruces, NM, October 1979, pp. 3.1–3.20.
22. K.-L. Wong, *Compact and Broadband Microstrip Antennas*, Wiley, New York, 2002.
23. K.-L. Wong, *Planar Antennas for Wireless Communications*, Wiley, New York, 2003.

24. R. B. Waterhouse, S. D. Targonski, and D. M. Kokotoff, Design and performance of small printed antennas, *IEEE Transactions on Antennas and Propagation*, vol. AP-46, no. 11, November 1998, pp. 1629–1633.
25. R. B. Waterhouse, ed., *Microstrip Patch Antennas: A Designer's Guide*, Kluwer Academic, Boston, 2003.
26. T. Taga and K. Tsunekawa, Performance analysis of a built-in planar inverted-F antenna for 800 MHz band portable radio units, *IEEE Transactions on Selected Areas in Communication*, vol. SAC-5, no. 5, June 1987, pp. 921–929.
27. R. B. Waterhouse, Design of probe-fed stacked patches, *IEEE Transactions on Antennas and Propagation*, vol. AP-47, no. 12, December 1999, pp. 1780–1784.
28. S. D. Targonski, R. B. Waterhouse, and D. M. Pozar, Design of wide-band aperture-stacked patch microstrip antennas, *IEEE Transactions on Antennas and Propagation*, vol. AP-46, no. 9, September 1998, pp. 1245–1251.
29. S. D. Targonski and R. B. Waterhouse, Reflector elements for aperture and aperture coupled microstrip antennas, *IEEE Antennas and Propagation Symposium Digest*, Montreal, Quebec, Canada, July 1997, pp. 1840–1843.
30. J. R. Sanford and A. Tengs, A two substrate dual polarized aperture coupled patch, *IEEE Antennas and Propagation Symposium Digest*, 1996, pp. 1544–1547.
31. T. Metzler, Microstrip series arrays, *Proceedings of the Workshop on Printed Circuit Antennas*, New Mexico State University, Las Cruces, NM, October 1979, pp. 20.1–20.16.
32. B. B. Jones, F. V. M. Chow, and A. W. Seeto, The synthesis of shaped patterns with series-fed microstrip patch arrays, *IEEE Transactions on Antennas and Propagation*, vol. AP-30, no. 6, November 1982, pp. 1206–1212.
33. D. A. Huebner, An electrically small dipole planar array, *Proceedings of the Workshop on Printed Circuit Antennas*, New Mexico State University, Las Cruces, NM, October 1979, pp. 17.1–17.16.
34. R. S. Elliott and G. J. Stern, The design of microstrip dipole arrays including mutual coupling, parts I and II, *IEEE Transactions on Antennas and Propagation*, vol. AP-29, no. 5, September 1981, pp. 757–765.
35. K. Solbach, Microstrip-Franklin antenna, *IEEE Transactions on Antennas and Propagation*, vol. AP-30, no. 4, July 1982, pp. 773–775.
36. I. J. Bahl et al., Design of microstrip antennas covered with a dielectric layer, *IEEE Transactions on Antennas and Propagation*, vol. AP-30, no. 2, March 1982, pp. 314–318.